Special Techniques of Digital Holography

OSA DH 2012
Tutorial Presentation
May 1, 2012

M.K. 'Paul' Kim, Professor
Digital Holography and Microscopy Laboratory
Dept. of Physics
University of South Florida
Tampa, FL 33647
mkkim@usf.edu
http://faculty.cas.usf.edu/mkkim/

Holography

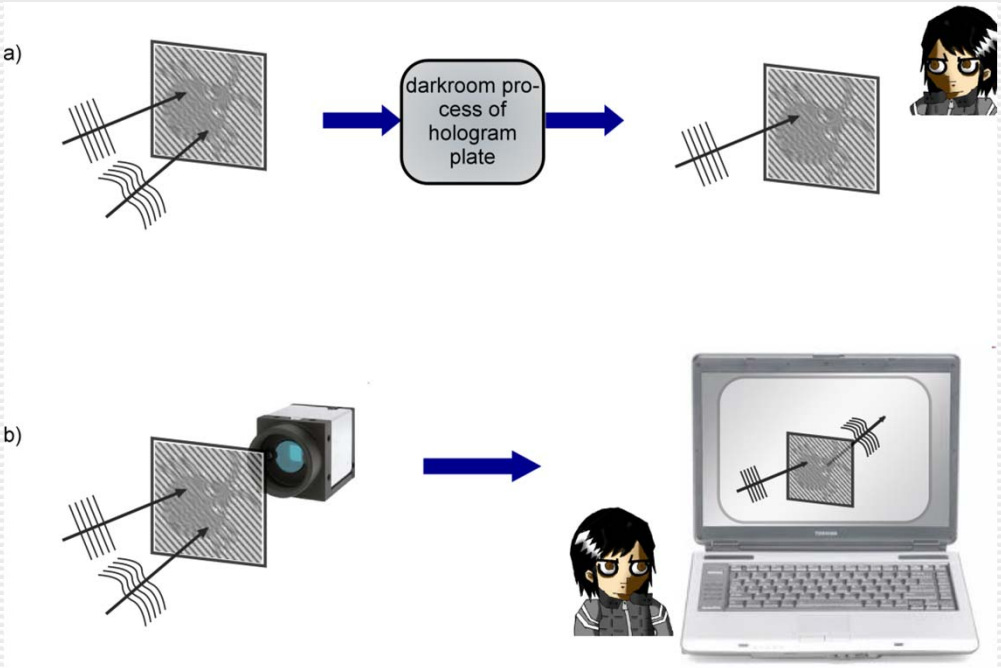

- Generation of holographic interference by superposition of object and reference waves
- Reconstruction of holographic image by illumination of the hologram with another reference wave

- Real space holography: optical generation & optical reconstruction
- Computer generated holography (CGH): numerical generation & optical reconstruction
- Digital holography (DH): optical generation & numerical reconstruction

Digital holographic microscopy process

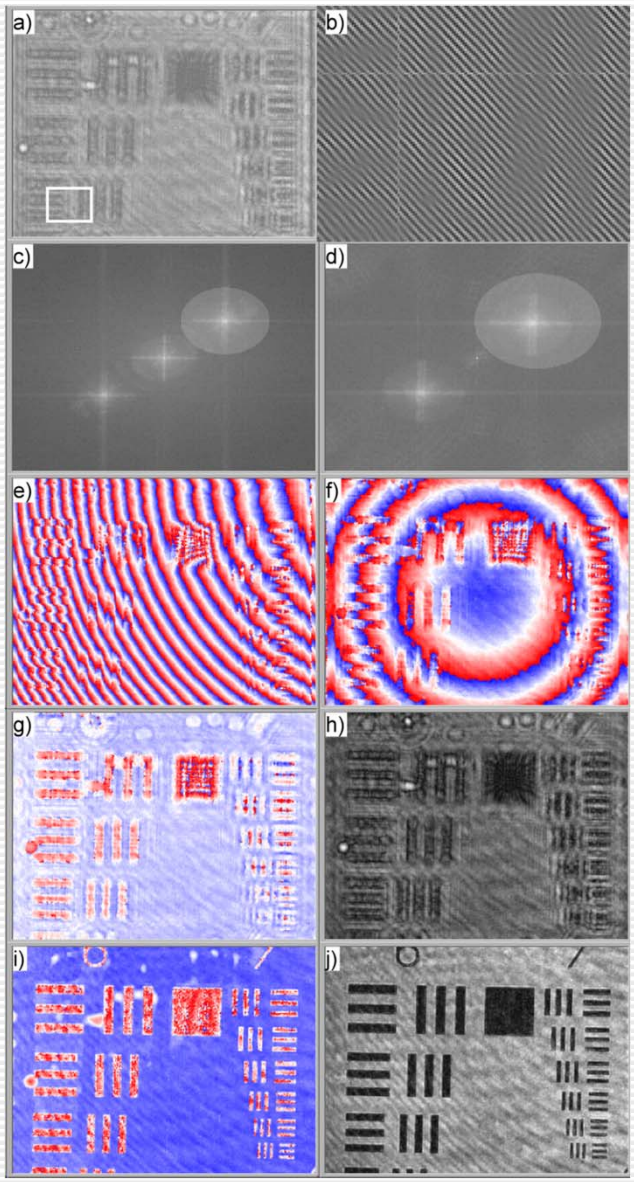

hologram

angular spectrum

tilt & curvature correction

complex hologram

complex image

a) Hologram

b) a detail of the small white rectangle in a)

c) angular spectrum including zero-order terms

d) angular spectrum after subtraction of object and reference intensities from the hologram, with the brighter circular area for band-pass filter

e) reconstructed phase profile at hologram plane, without any corrections

f) phase profile after correct centering of the filtered angular spectrum

g) phase profile after compensation of the spherical wave curvature

h) the amplitude image at the hologram plane corresponding to the phase image g)

i) phase image after numerical propagation to the object focus distance

j) the focused amplitude image

DH QPM: SKOV-3 ovarian cancer cells

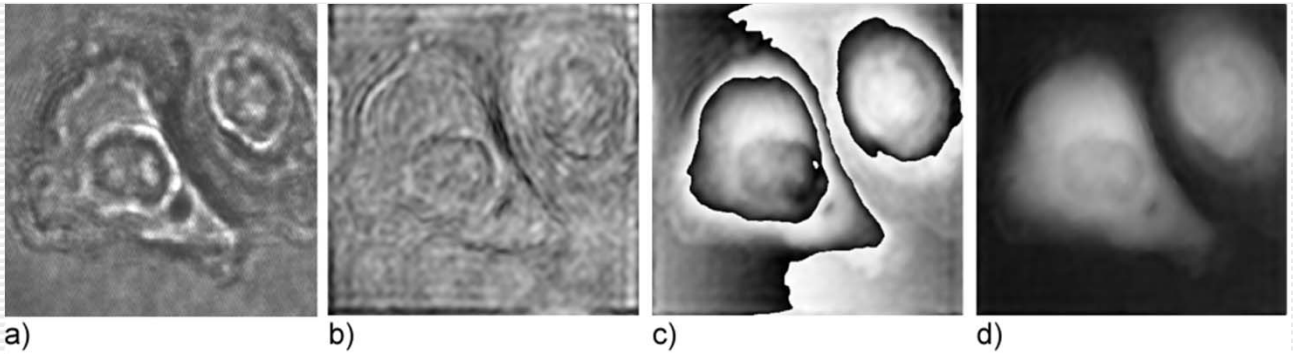

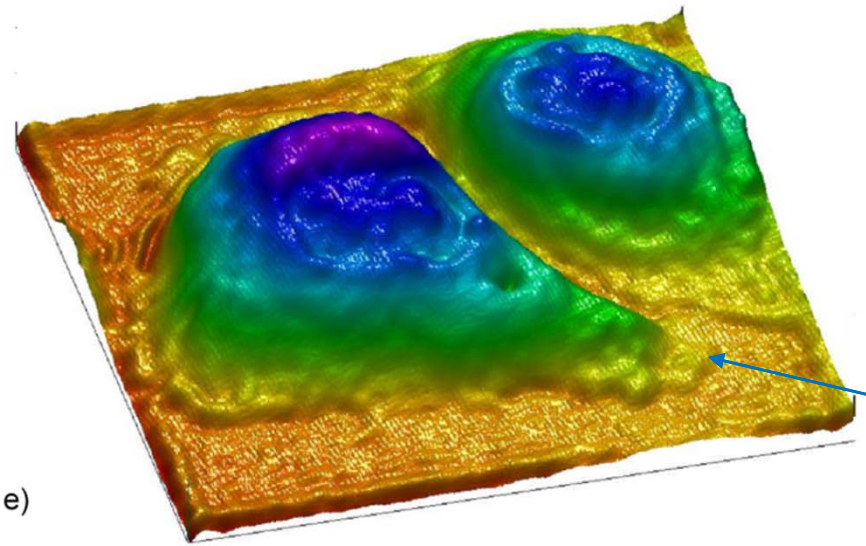

60 x 60μm^2
(404 x 404 pixels)
z = 5μm

a) hologram
b) amplitude image
c) phase image
d) unwrapped phase image
e) pseudo-3D pseudo-color

Lamellipodia
thickness=320nm

Optical Thickness of cells ~2.8μm

[C. J. Mann, L. F. Yu, C. M. Lo, and M. K. Kim, Optics Express 13, 8693-8698 (2005).]

optical phase unwrapping

- J. Gass, A. Dakoff, and M. K. Kim, "Phase imaging without 2-pi ambiguity by mult-iwavelength digital holography," Opt. Lett. **28,** 1141-1143 (2003)

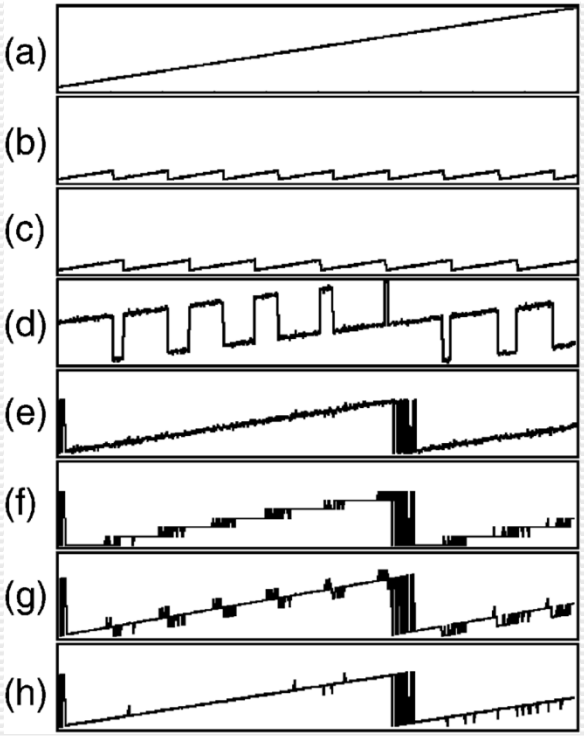

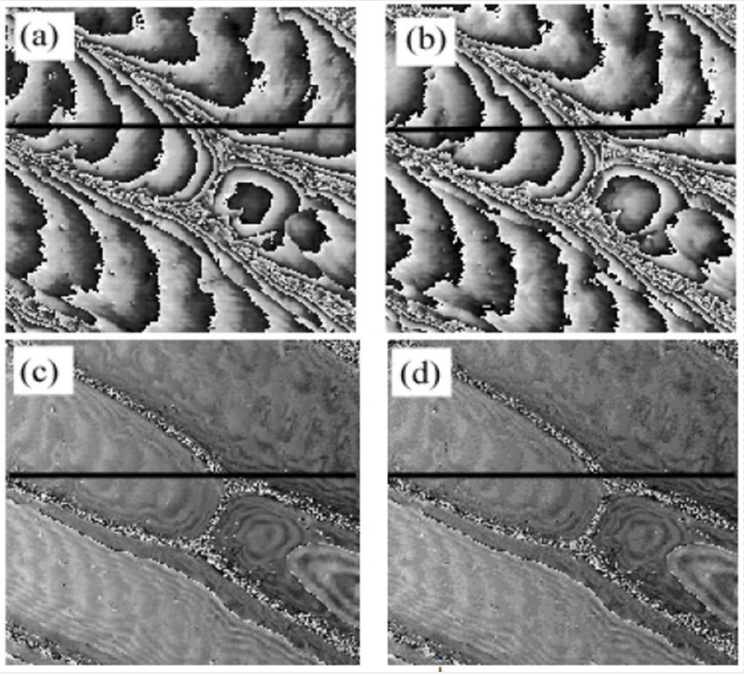

Fig. 9.6: Optical phase unwrapping. a) Height profile $z(x)$ of a slanted plane of maximum height 5 μm; b) and c) phase profiles $\varphi_1(x,y)$ and $\varphi_2(x,y)$ with $\lambda_1 = 0.532$ μm and $\lambda_2 = 0.633$ μm, respectively; d) $\Delta\varphi = \varphi_1 - \varphi_2$; e) add 2π wherever $\Delta\varphi < 0$; f) $\text{int}\left[\Phi'_{12}\Lambda_{12}/\lambda_1\right]\cdot 2\pi$; g) $\Phi_{12} = \varphi_1 + \text{int}\left[\Phi'_{12}\Lambda_{12}/\lambda_1\right]\cdot 2\pi$; h) clean up glitches by adding or subtracting λ_1 if $\left|\Phi_{e)} - \Phi_{g)}\right| \geq \lambda_1/2$ [19].

optical phase unwrapping

- A. Khmaladze, A. Restrepo-Martinez, M. Kim, R. Castaneda, and A. Blandon, Appl. Opt. 47, 3203-3210 (2008).]

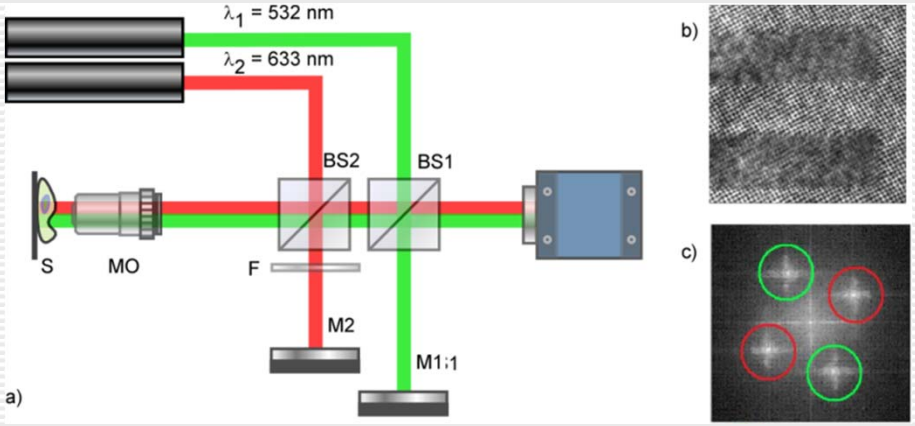

Two-wavelength holographic interferometer.

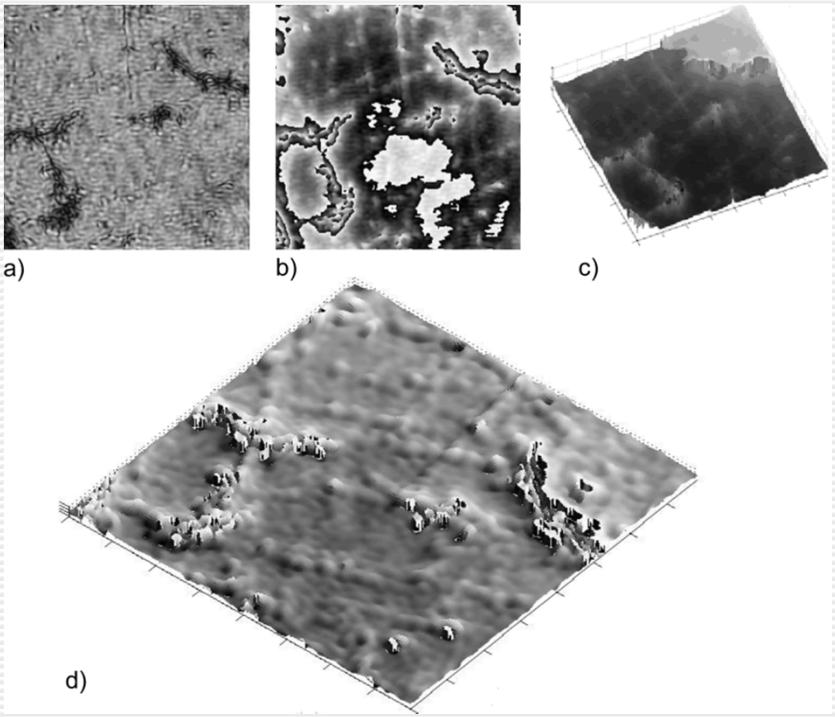

Two-wavelength optical phase unwrapping on images of a porous coal sample.

super-resolution by synthetic aperture

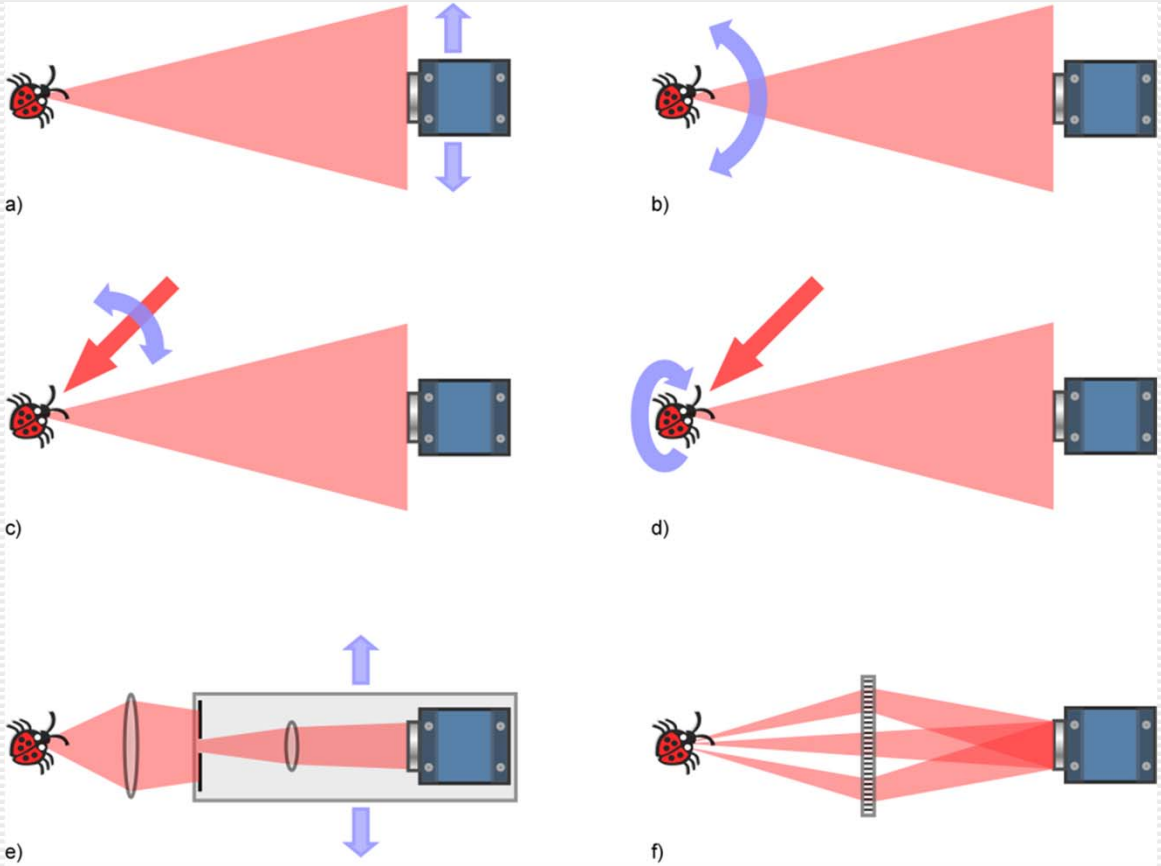

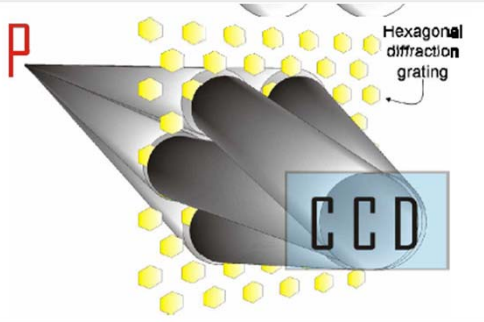

Methods for aperture synthesis.

a) Translate the camera;

b) tilt the object plane;

c) scan the illumination angle;

d) rotate the object;

e) scan across the Fourier plane;

f) use a diffraction grating

hexagonal grating [M. Paturzo, F. Merola, S. Grilli, S. De Nicola, A. Finizio, and P. Ferraro, Optics Express 16, 17107-17118 (2008)]

super-resolution by synthetic aperture

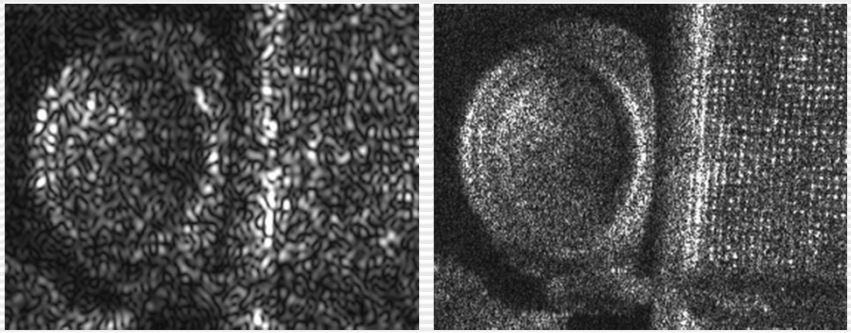

3x3 camera scan
[J. H. Massig, Optics Letters 27, 2179-2181 (2002)]

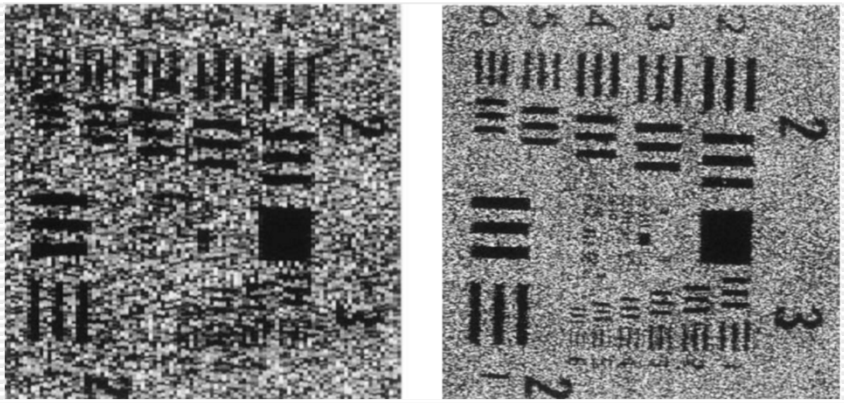

Fourier domain scan
[F. Le Clerc, M. Gross, and L. Collot, Optics Letters 26, 1550-1552 (2001).]

multi-mode imaging

- C. Liu, Y. S. Bae, W. Z. Yang, and D. Y. Kim, "All-in-one multifunctional optical microscope with a single holographic measurement," Optical Engineering **47,** 087001 (2008).

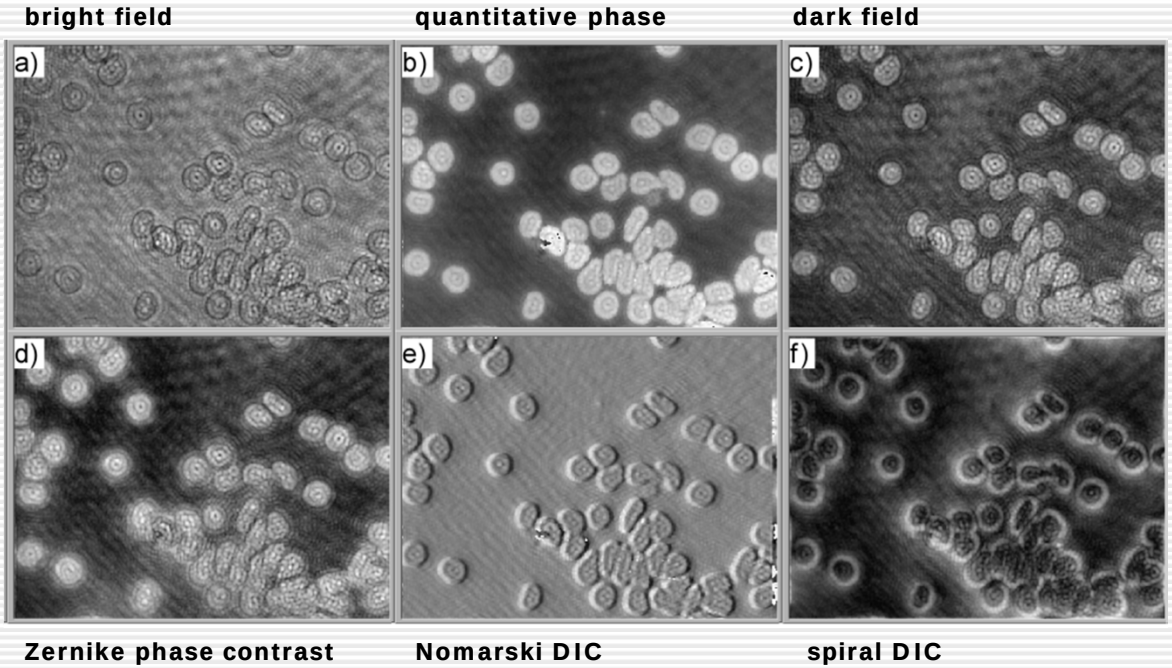

Multi-mode contrast generation from a single hologram of red blood cells.
a) amplitude contrast;
b) quantitative phase contrast;
c) dark field;

$$1-\delta\left(k_x,k_y\right)$$

d) Zernike phase contrast;

$$1-(1-i)\delta\left(k_x,k_y\right)$$

e) DIC;

$$\exp\left[2\pi i\left(k_x\Delta_x+k_y\Delta_y\right)\right]$$

f) spiral DIC

$$\exp(i\theta)$$

dark field

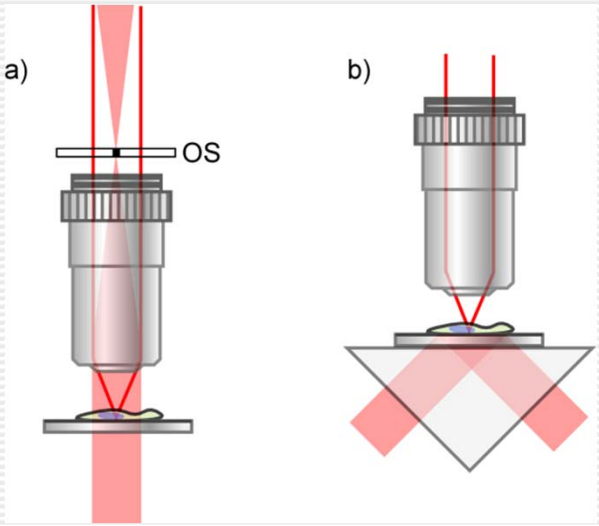

Dark field illumination for DHM.

a) An optical stop (OS) placed at the back focal plane of the objective
[F. Dubois, and P. Grosfils, "Dark-field digital holographic microscopy to investigate objects that are nanosized or smaller than the optical resolution," Optics Letters 33, 2605-2607 (2008)];

b) use of the evanescent field of TIR
[N. Warnasooriya, F. Joud, P. Bun, G. Tessier, M. Coppey-Moisan, P. Desbiolles, M. Atlan, M. Abboud, and M. Gross, "Imaging gold nanoparticles in living cell environments using heterodyne digital holographic microscopy," Optics Express 18, 3264-3273 (2010)].

dark field + heterodyne DH

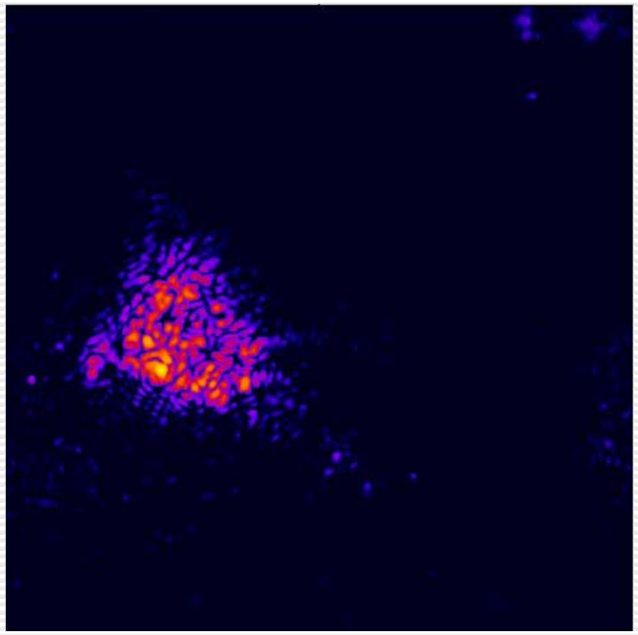

Fibroblast cell tagged with a 40 nm gold particle. Reconstructed Holographic intensity *I* image. The 40 nm gold particle is marked with a white arrow. (512×512×512 voxels; voxel size 177 nm in all directions). The holographic reconstruction is made from 1 CCD frame with an exposure time of 100 ms.

TIRHM: total internal reflection holographic microscopy

- W. M. Ash, and M. K. Kim, "Digital holography of total internal reflection," Optics Express **16,** 9811-9820 (2008).

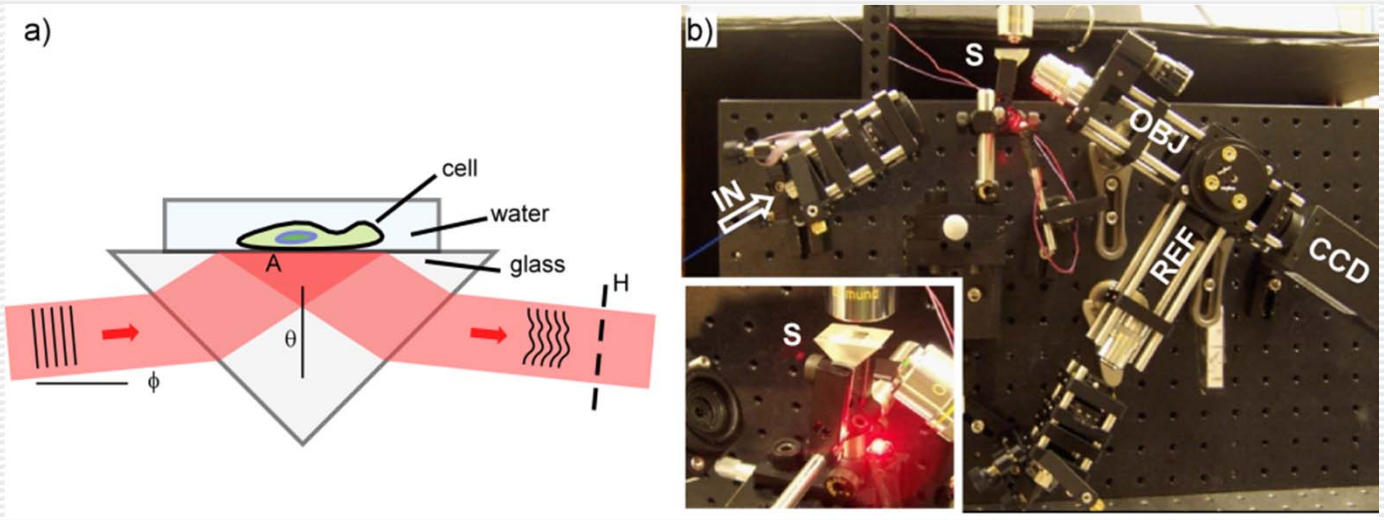

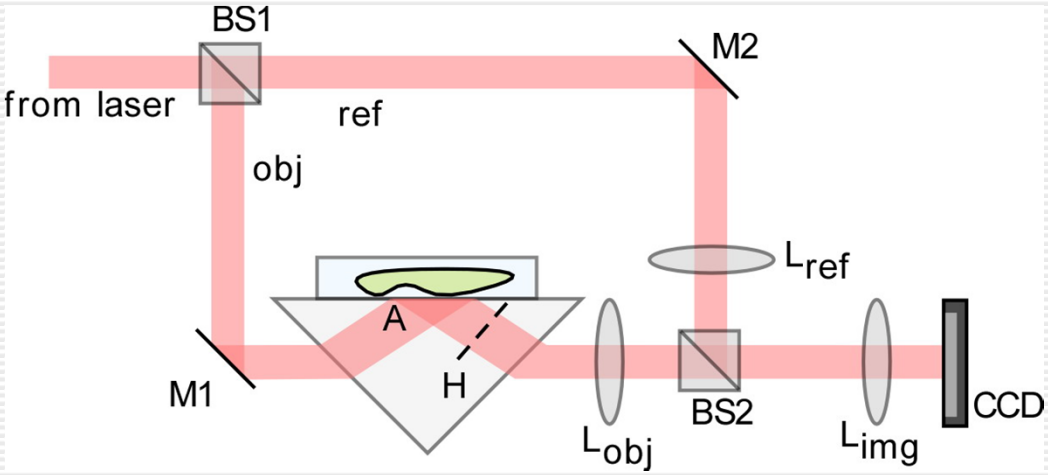

TIRHM: total internal reflection holographic microscopy

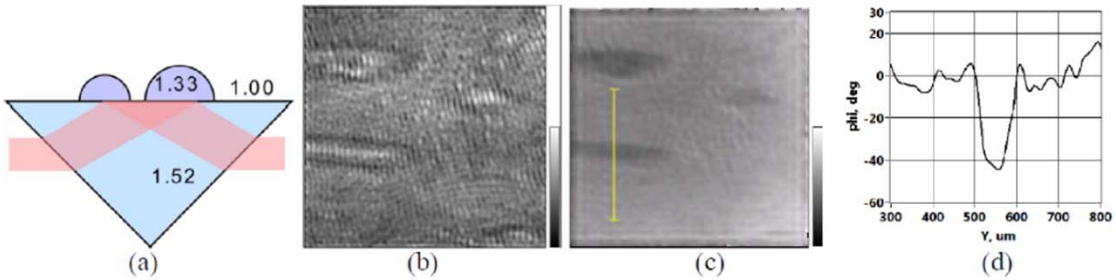

Fig. 5. a) General configuration of water droplets placed on prism. b) Amplitude and c) phase images of light reflected from the prism. Field of view is approximately 300 x 900 μm^2 with 256 x 256 pixels. Gray scale for b) is 0 ~ 1 in arbitrary unit, while for c) it is -180° ~ $+180^\circ$. d) Graph of cross-section along a vertical line through a water drop in c). e) A similar graph for a droplet of 50/50 mixture of water and ethylene glycol.

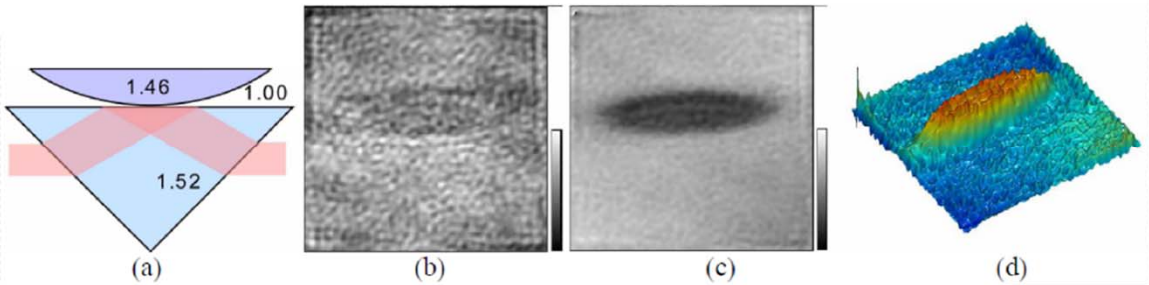

Fig. 6. a) General configuration of quartz lens placed on prism. b) Amplitude and c) phase images of light reflected from the prism. d) Pseudo-color perspective rendering of c). Field of view is approximately 260 x 780 μm^2 with 256 x 256 pixels. Gray scale for b) is 0 ~ 1 in arbitrary unit, while for c) it is -180° ~ $+180^\circ$.

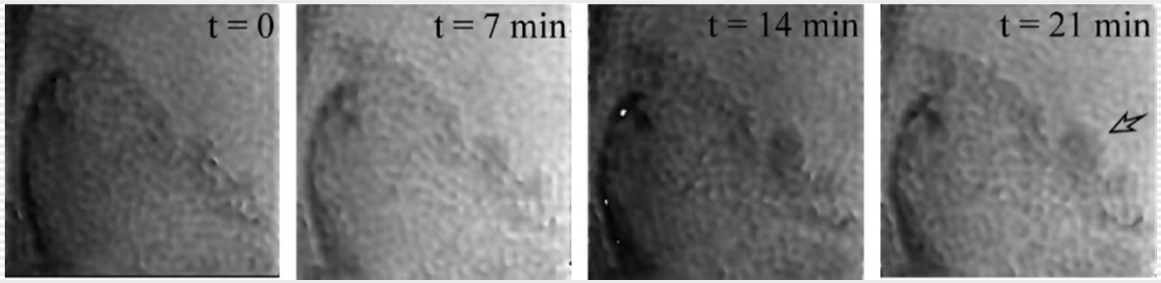

TIRHM images of *amoeba proteus* pseudopod activity

color

- color holography
- multi-wavelength holographic processing

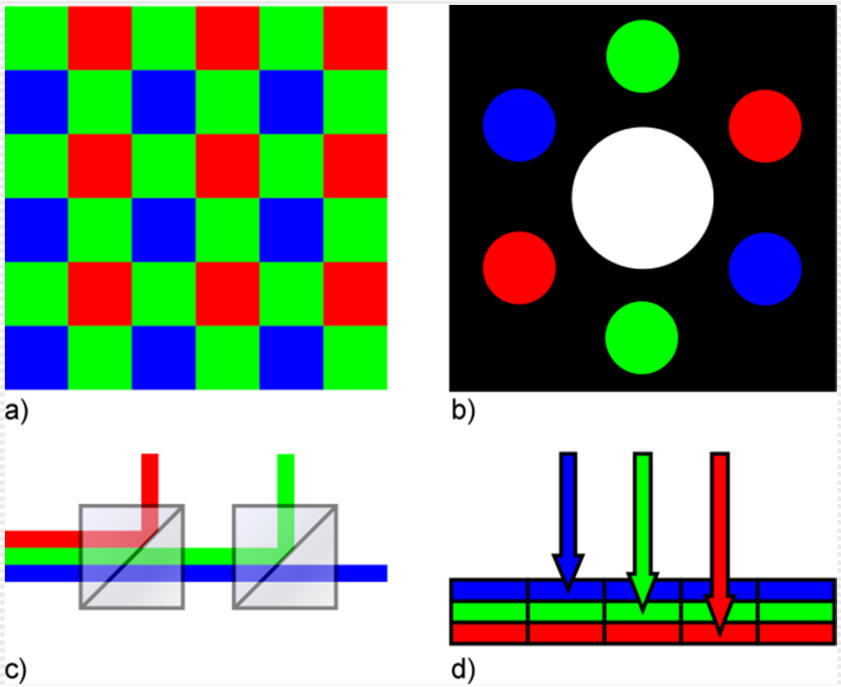

Methods to acquire the three color channels simultaneously.
a) Bayer color mosaic on CCD sensor array;
b) angular multiplexing;
c) use of dichroic beam splitters and separate cameras;
d) stacked photodiode sensors.
[P. Tankam, P. Picart, D. Mounier, J. M. Desse, and J. C. Li, Applied Optics 49, 320-328 (2010)]

color

- color holography
- multi-wavelength holographic processing

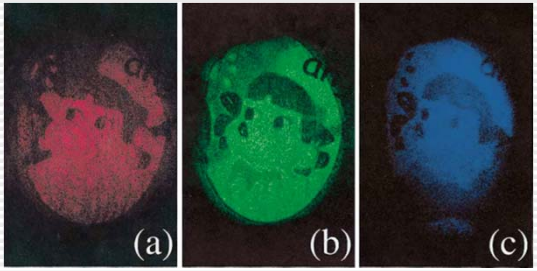

HeCd laser: 636.0, 537.8, 441.6 nm

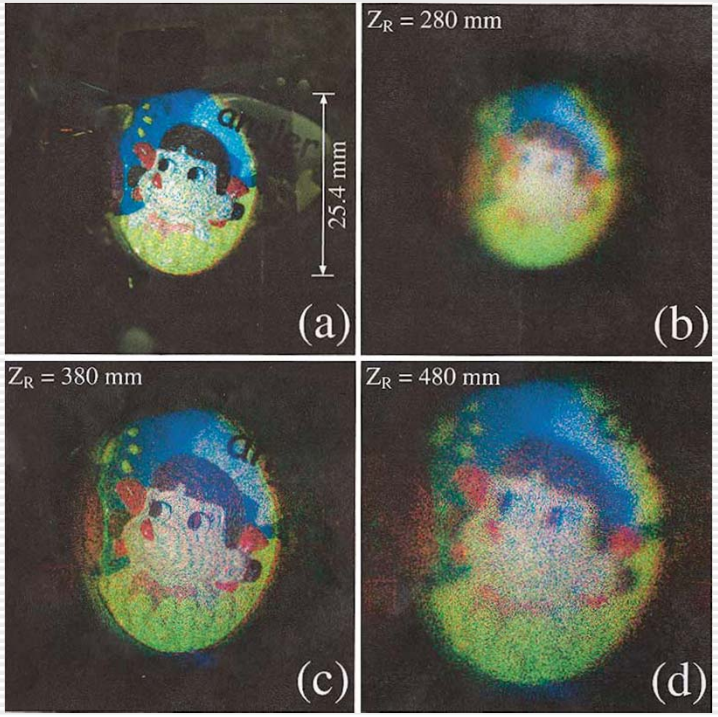

(a) ordinary image taken by the color CCD camera with an imaging lens. Unified images reconstructed at (b) *Z* 280 mm, (c) *Z* 380 mm, and (d) *Z* 480 mm.
[J. Kato, I. Yamaguchi, and T. Matsumura, "Multicolor digital holography with an achromatic phase shifter," Optics Letters 27, 1403-1405 (2002)]

THz (680, 725 GHz duel wavelength OPU)

- MS Heimbeck, MK Kim, DA Gregory, & HO Everitt, Opt. Express 19 9192 (2011)

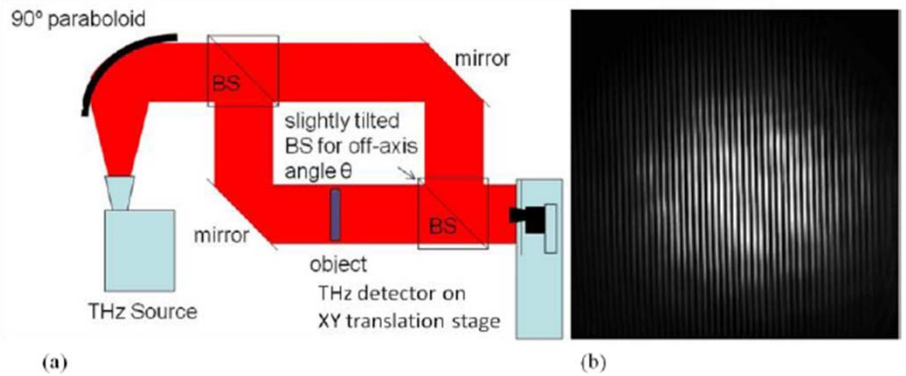

Fig. 1. THz digital holography experimental configuration (a) and a typical interferogram at detector/hologram recording plane (b).

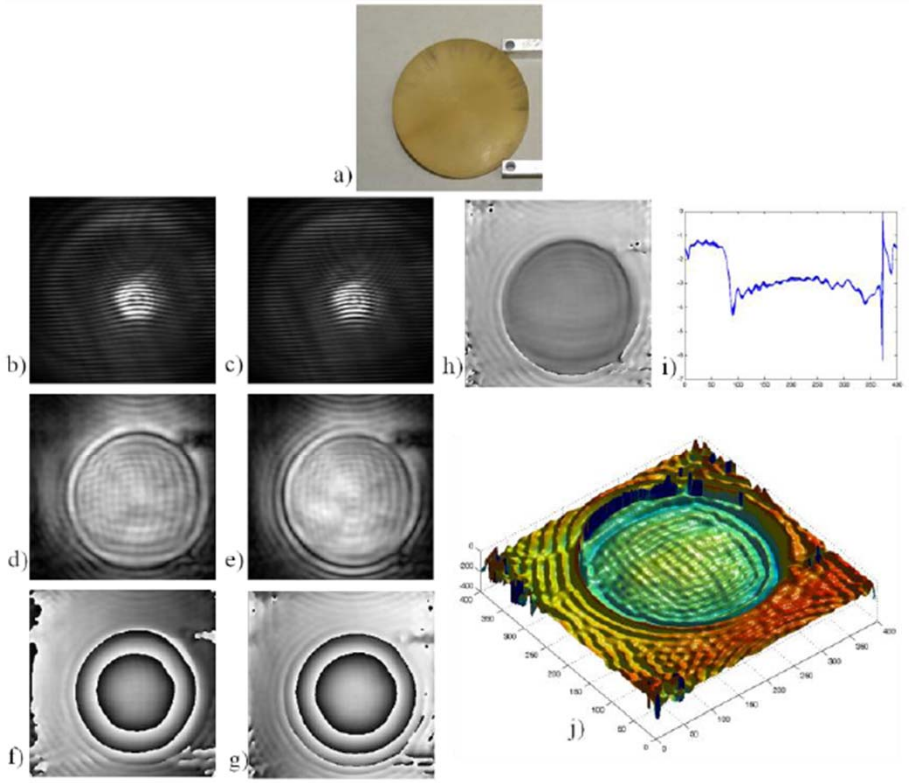

Fig. 6. Steps in the reconstruction of the phase object using dual wavelength reconstruction: photograph (a), holograms at 680 and 725 GHz (b-c), amplitude reconstructions (d-e), phase reconstructions (f-g), unwrapped reconstruction (h), cross-section through center of unwrapped reconstruction (i), pseudo 3D perspective of the unwrapped reconstruction (j).

X-ray

- [S. Eisebitt, J. Luning, W. F. Schlotter, M. Lorgen, O. Hellwig, W. Eberhardt, and J. Stohr, Nature 432, 885-888 (2004).]

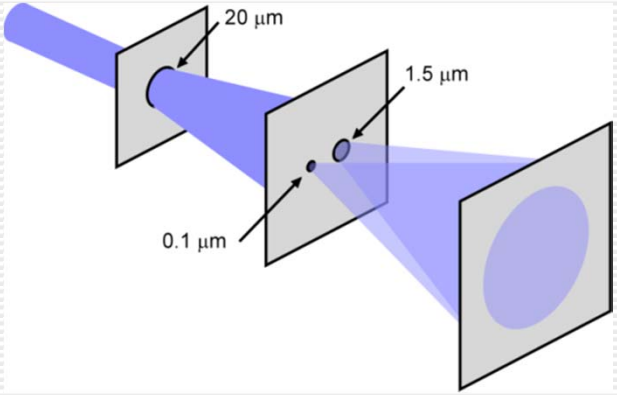

Digital Fourier holography of 1.59 nm X-ray. Lithographically manufactured mask contains 1.5 mm sample (magnetic film) aperture and 0.1 mm reference aperture.

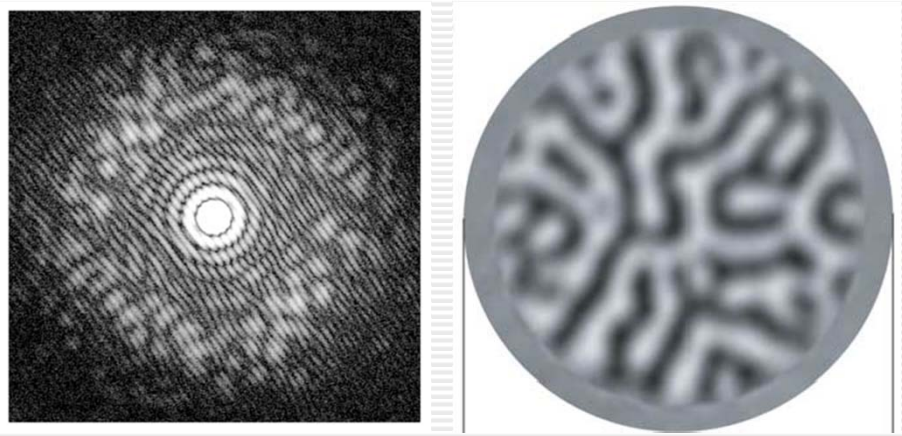

Hologram recorded with X-rays (right circular polarization) at a wavelength of 1.59 nm.

digital holography of nonlinear optics

- digital holography of light-induced refractive index change
  - [S. Grilli, P. Ferraro, M. Paturzo, D. Alfieri, and P. De Natale, "In-situ visualization, monitoring and analysis of electric field domain reversal process in ferroelectric crystals by digital holography," Optics Express **12,** 1832-1842 (2004).]
- digital holography of NLO light
  - [E. Shaffer, N. Pavillon, J. Kuhn, and C. Depeursinge, "Digital holographic microscopy investigation of second harmonic generated at a glass/air interface," Optics Letters **34,** 2450-2452 (2009)]
- imaging through NLO material by digital holography
  - [C. Barsi, W. J. Wan, and J. W. Fleischer, "Imaging through nonlinear media using digital holography," Nat. Photonics **3,** 211-215 (2009)]

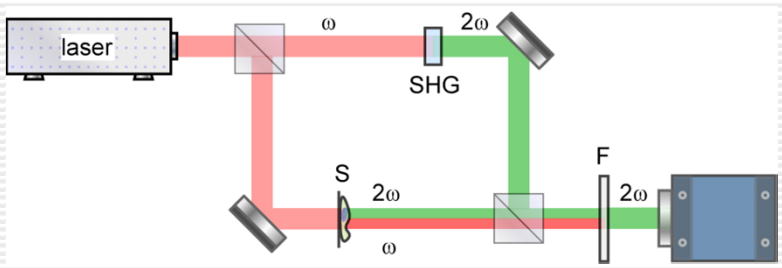

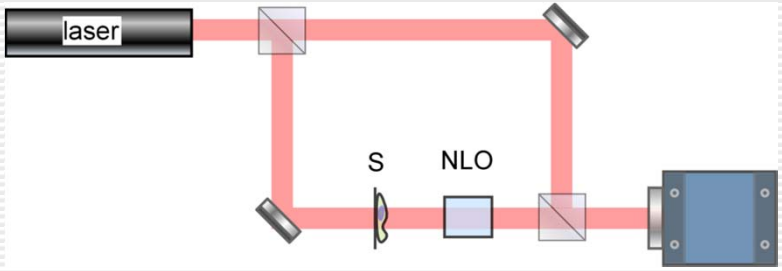

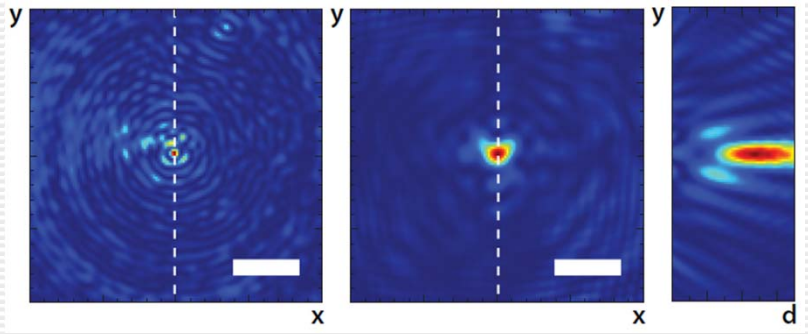

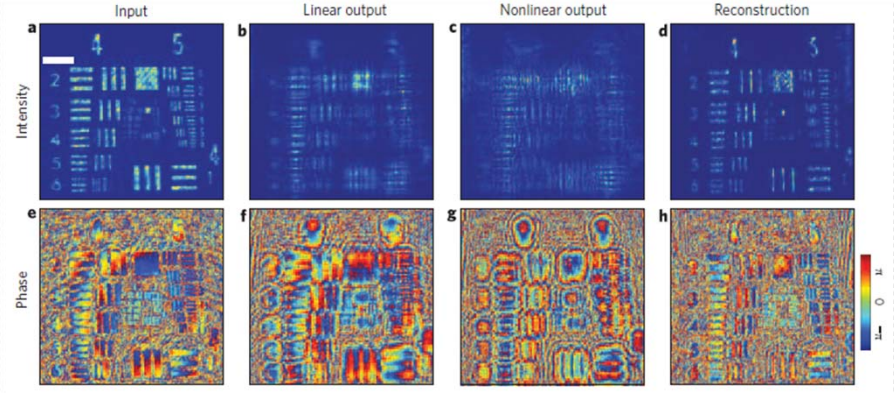

PSDH: phase shifting digital holography

- I. Yamaguchi, and T. Zhang, "Phase-shifting digital holography," Optics Letters **22,** 1268-1270 (1997).

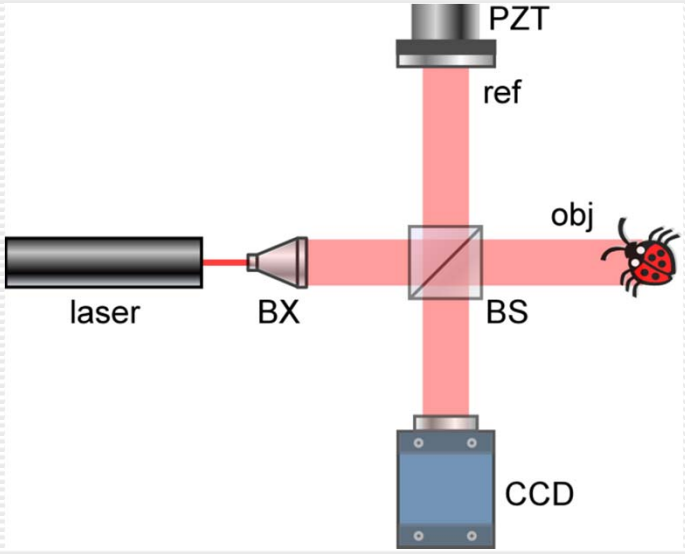

Phase shifting digital holography with Michelson interferometer. BX: beam expander; BS: beam splitter; PZT: piezo-mounted reference mirror.

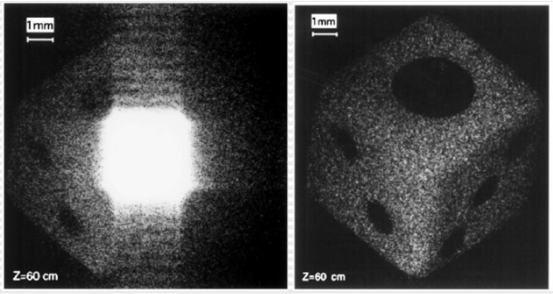

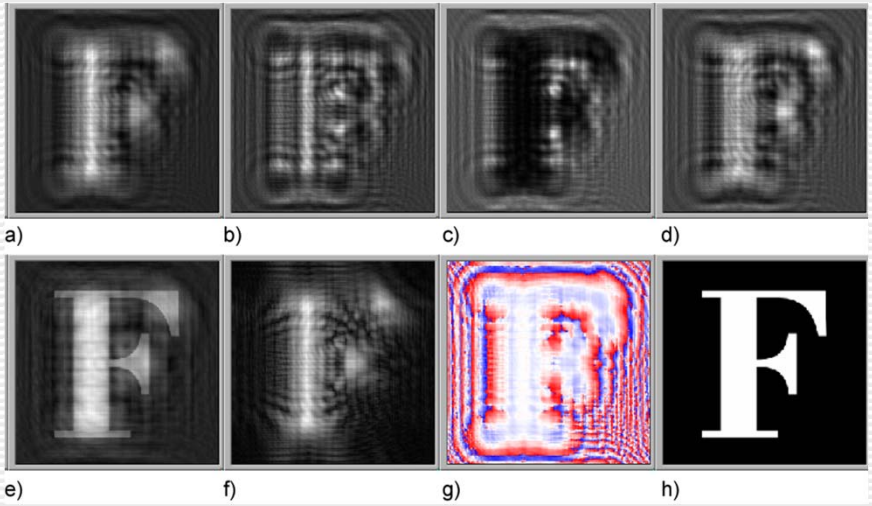

Simulation of PSDH. a) I_0; b) $I_{\pi/2}$; c) I_π; d) $I_{3\pi/2}$; e) image reconstructed from I_0; f) $\sqrt{E_o^2(x,y)}$; g) $\varphi(x,y)$; h) image reconstructed from $\sqrt{E_o^2}\exp[i\varphi]$.

$$I_\varphi(x,y) = \left|E_R e^{i\varphi} + E_O\right|^2$$

$$= I_R + I_O + E_R e^{i\varphi} E_O^* + E_R^* e^{-i\varphi} E_O$$

$$E_O(x,y) = \frac{1}{4E_R}\left[\left(I_0 - I_\pi\right) + i\left(I_{3\pi/2} - I_{\pi/2}\right)\right]$$

PSDH

- three-step & two-step methods
- unknown phase stepts
- heterodyne DH
- parallel PS
- fractional Talbot effect
- spatial phase shifting

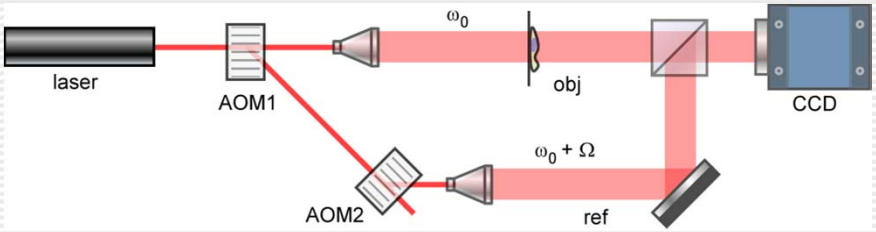

[F. Le Clerc, L. Collot, and M. Gross, "Numerical heterodyne holography with two-dimensional photodetector arrays," Optics Letters 25, 716-718 (2000)]

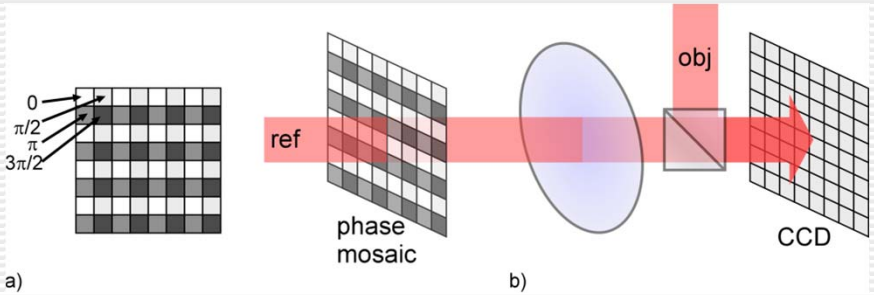

[Y. Awatsuji, T. Tahara, A. Kaneko, T. Koyama, K. Nishio, S. Ura, T. Kubota, and O. Matoba, "Parallel two-step phase-shifting digital holography," Applied Optics 47, D183-D189 (2008)]

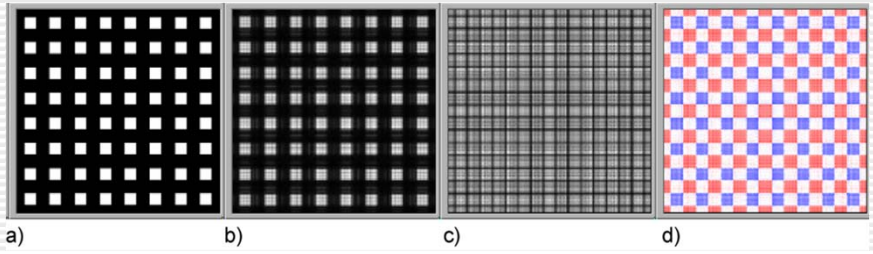

[L. Martinez-Leon, M. Araiza, B. Javidi, P. Andres, V. Climent, J. Lancis, and E. Tajahuerce, "Single-shot digital holography by use of the fractional Talbot effect," Optics Express 17, 12900-12909 (2009)]

low coherence holography

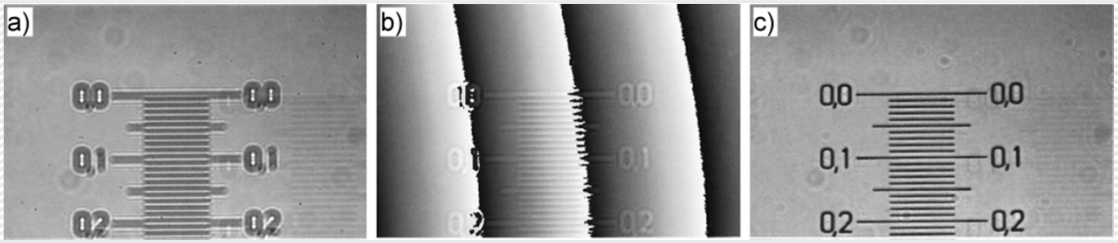

Example of refocusing capability with a digital holography microscope on a metric scale (100 divisions/mm). a) Intensity of the defocus; b) phase of the defocus image; c) computer-refocused image. The refocus distance is 80 mm.
[F. Dubois, L. Joannes, and J. C. Legros, "Improved three-dimensional imaging with a digital holography microscope with a source of partial spatial coherence," Applied Optics 38, 7085-7094 (1999)]

G. Pedrini, and H. J. Tiziani, "Short-coherence digital microscopy by use of a lensless holographic imaging system," Applied Optics 41, 4489-4496 (2002).

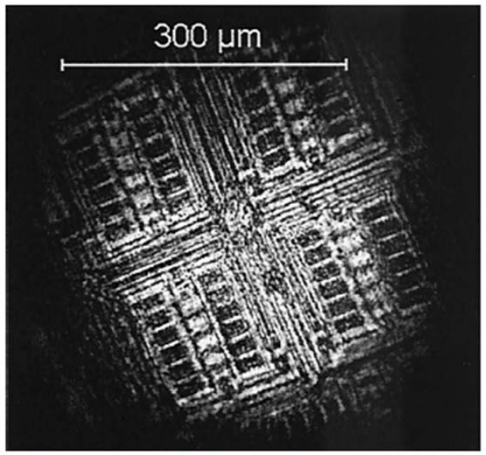

Fig. 6. Reconstruction of the image of a microcircuit recorded with a lensless short-coherence arrangement and reconstructed with the Rayleigh–Sommerfeld method.

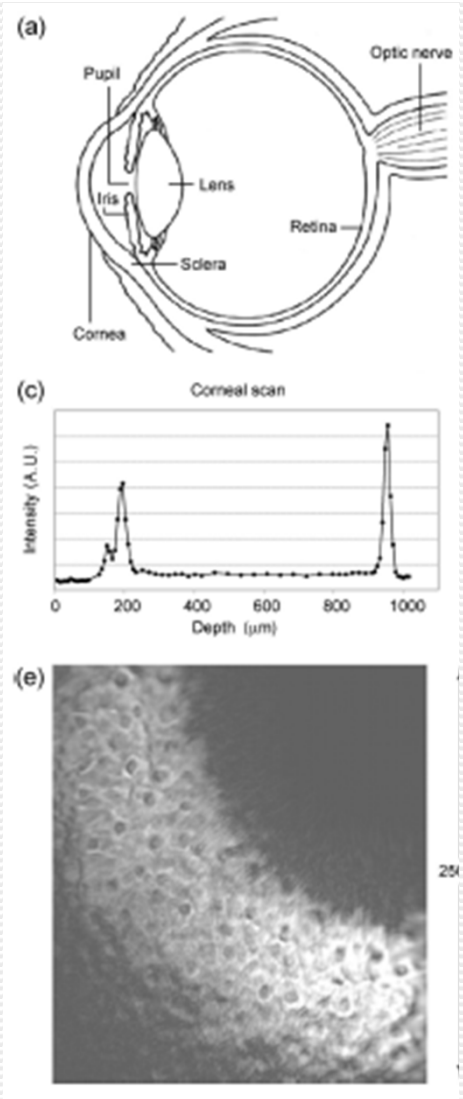

Sketches representing (a) the eye and (b) the cornea with its fine structure. (c) Backscattered intensity, obtained by scanning through the cornea. The double peak corresponds to the thick epithelium. The single peak to the right corresponds the endothelial monocellular layer. (d) Cross-sectional image of the whole cornea. The two interfaces of the epithelium are visible at the top of the image, and the endothelial layer is visible at the bottom. (e) *En face* image of porcine corneal epithelium *in situ*. This tomographic image yields details at the cellular level: image of nuclei and cytoplasm.
[P. Massatsch, F. Charriere, E. Cuche, P. Marquet, and C. D. Depeursinge, "Time-domain optical coherence tomography with digital holographic microscopy," Applied Optics 44, 1806-1812 (2005).]

FFOCT

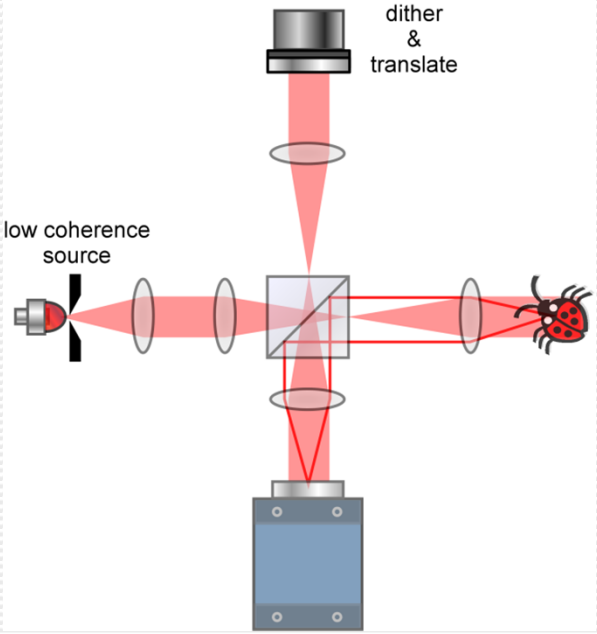

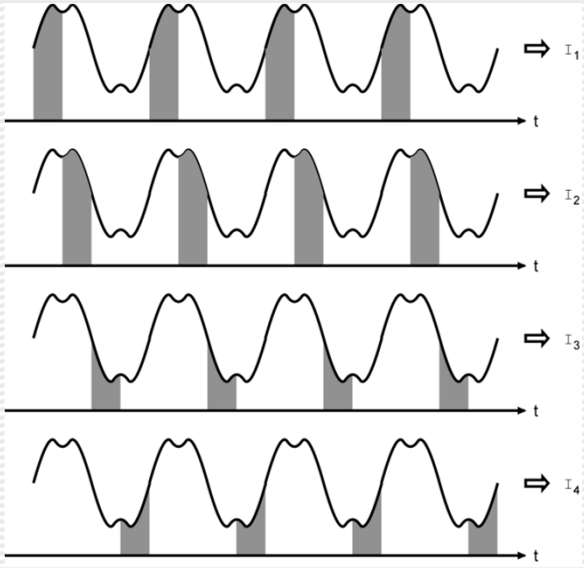

Synchronous illumination detection. The shaded areas represent the periods when the illumination is on and the graphs plot the intensity variation of a pixel as the reference mirror dithers sinusoidally. The intensity of the shaded areas is accumulated during a camera exposure and stored as one of the four phase-quadrature images.

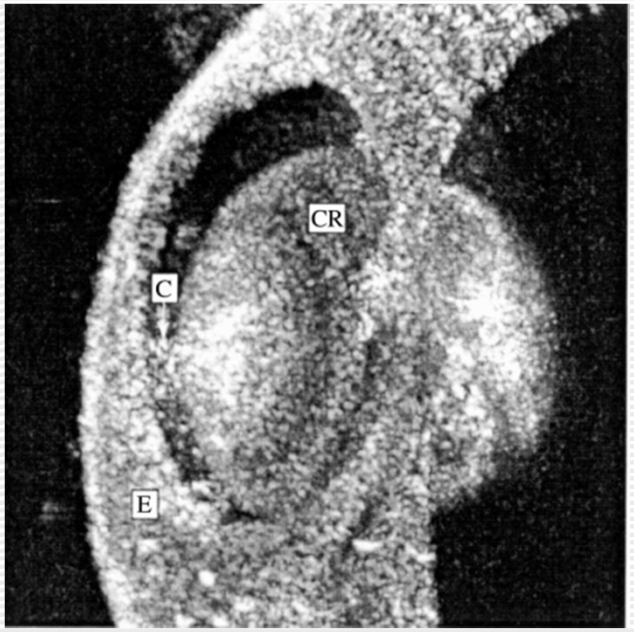

3D reconstruction of a Xenopus laevis tadpole eye by means of 300 tomographic images. The volume is 360 × 360 × 200 mm^3. E, exterior of the eye; C, cornea; CR, crystalline lens. [L. Vabre, A. Dubois, and A. C. Boccara, "Thermal-light full-field optical coherence tomography," Opt. Lett. 27, 530 (2002).]

color FFOCT

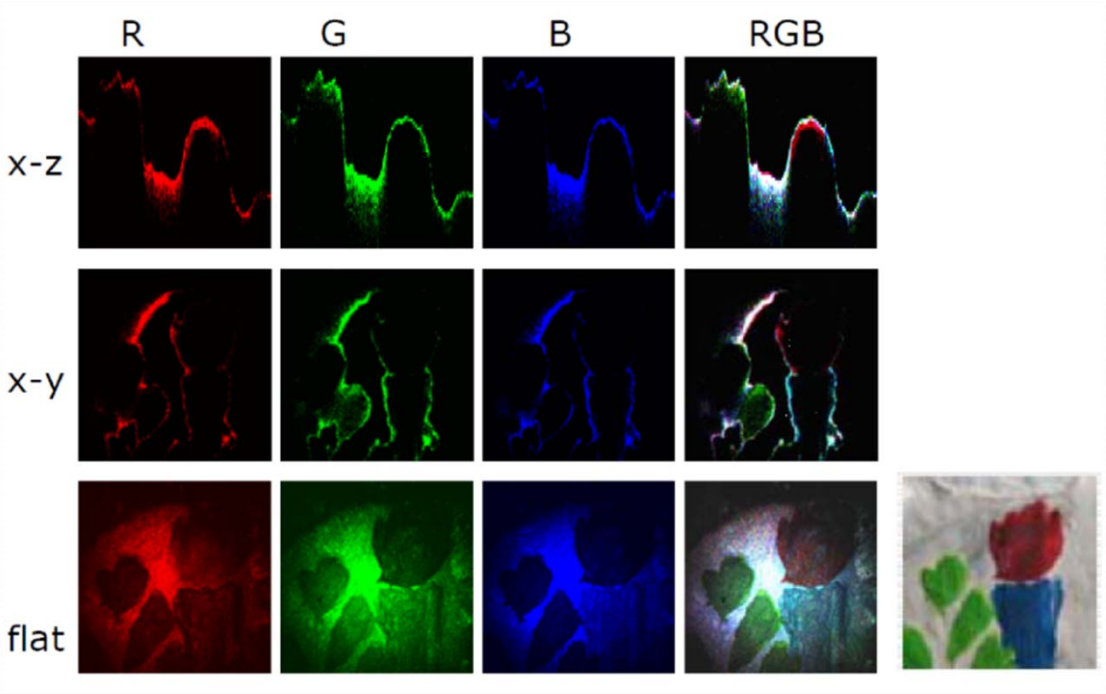

L. F. Yu, and M. K. Kim, "Full-color three-dimensional microscopy by wide-field optical coherence tomography," Optics Express 12, 6632-6641 (2004)

HOCI: holographic optical coherence imaging

- K. Jeong, J. J. Turek, and D. D. Nolte, "Fourier-domain digital holographic optical coherence imaging of living tissue," Applied Optics 46, 4999-5008 (2007).

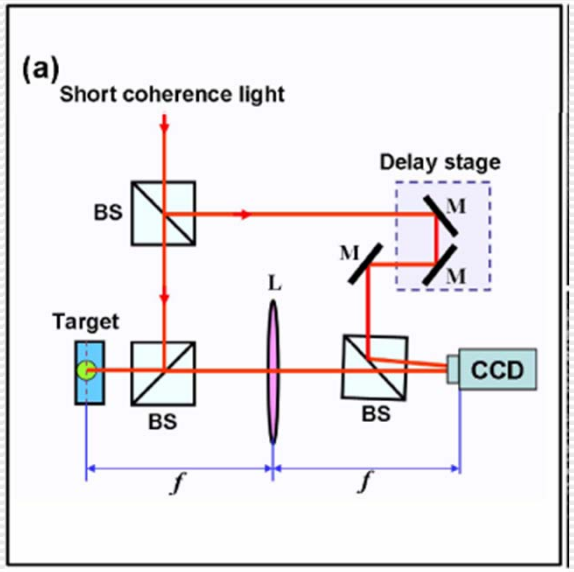

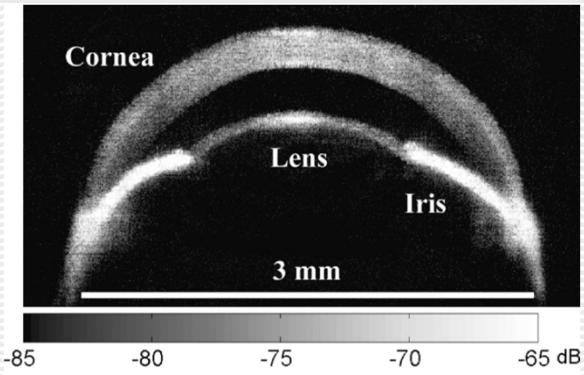

Mouse eye *in vitro* mosaic section of the anterior segment extracted from ten flythroughs.

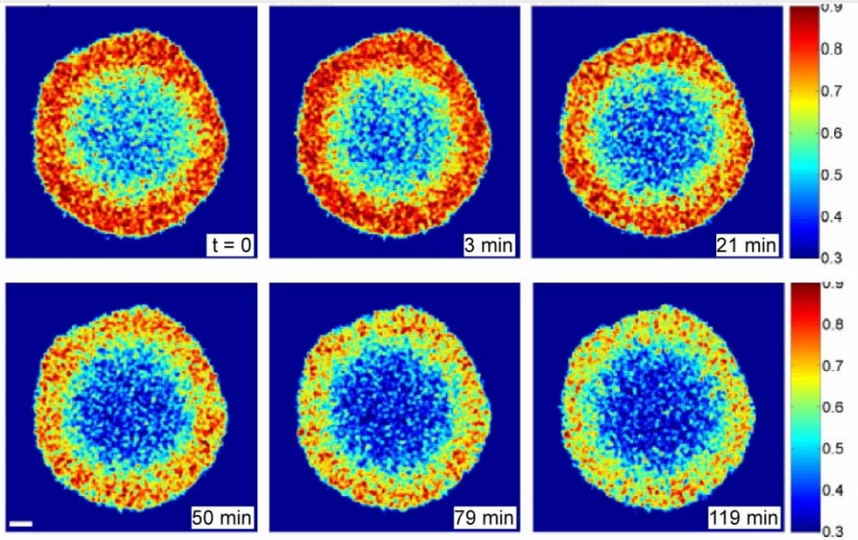

Motility maps showing the response of an 820-μm-diameter tumor (at a fixed depth of 350 μm from the tumor top) to 10 μg/ml nocodazole as a function of time (from healthy to 120 minutes later). Motility in the viable shell decreases with time, showing how nocodazole suppresses the activity of viable tumor cells. Bar, 100 μm.
[K. Jeong, J. J. Turek, and D. D. Nolte, "Volumetric motility-contrast imaging of tissue response to cytoskeletal anti-cancer drugs," Optics Express 15, 14057-14064 (2007)]

Rotating Ground Glass

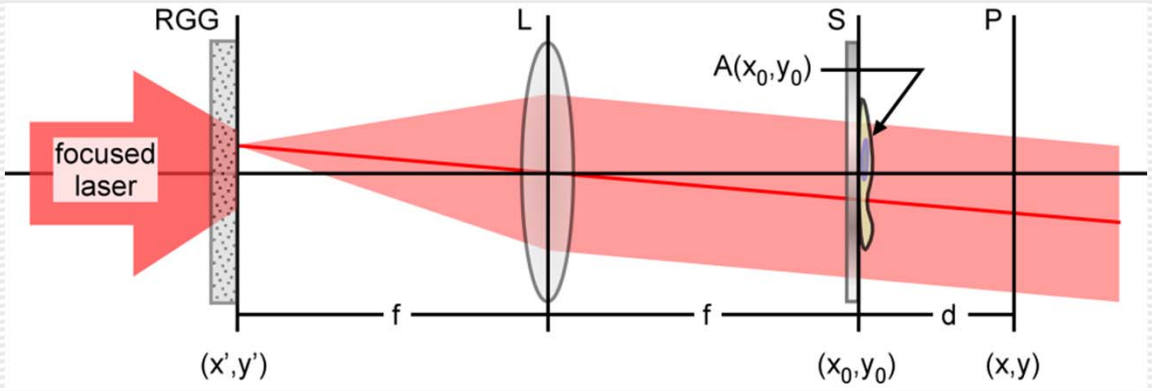

Geometry of partial coherence illumination. RGG: Rotating ground glass; L: condenser lens; S: sample plane; P: focus plane of the camera.

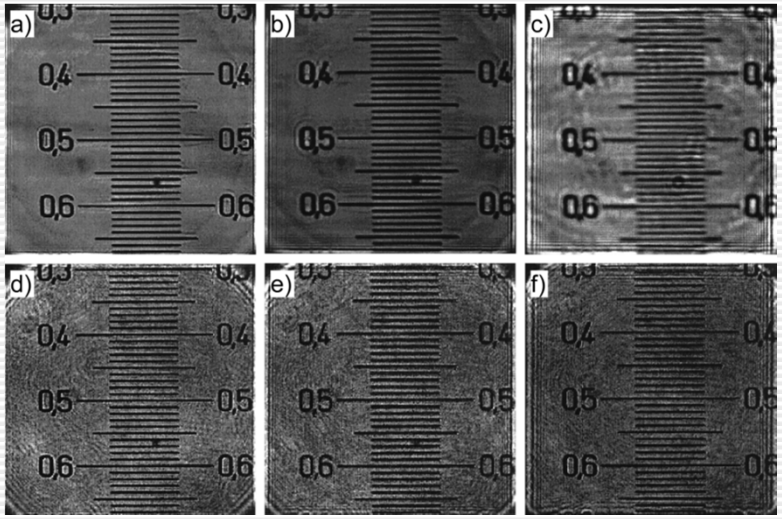

Refocusing property and spatial coherence. Panels a), b), and c) are with speckle size of 12 mm (low coherence), while d), e) and f) are with speckle size of 200 mm (high coherence). The refocus distances for each row are d = 50, 100, and 200 mm. [F. Dubois, M. L. N. Requena, C. Minetti, O. Monnom, and E. Istasse, "Partial spatial coherence effects in digital holographic microscopy with a laser source," Applied Optics 43, 1131-1139 (2004)]

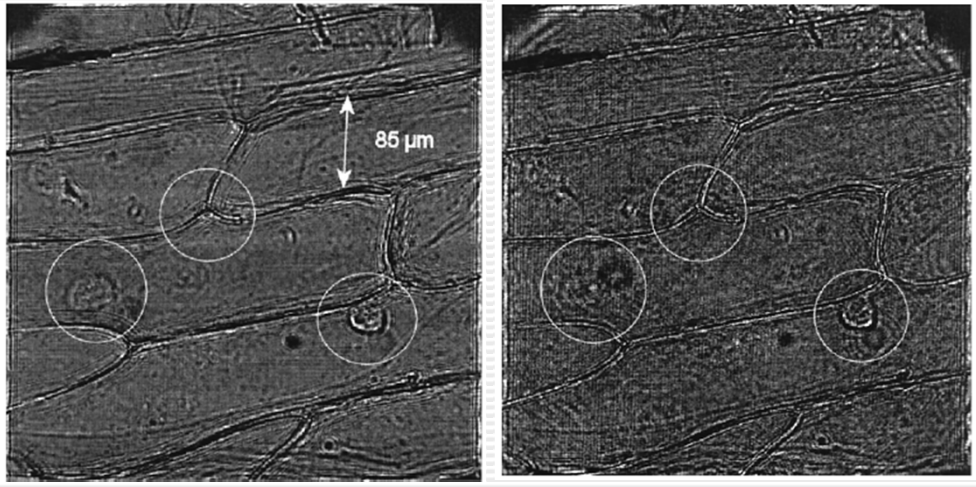

Fig. 4. Refocused onion peel image. (a) Refocusing distance d = 50 µm; speckle size σ = 12 µm. (b) Refocusing distance d = 50 µm; speckle size σ = 200 µm.

Lens-free on-chip holographic microscopy

- C. Oh, S. O. Isikman, B. Khademhosseinieh, and A. Ozcan, "On-chip differential interference contrast microscopy using lensless digital holography," Optics Express **18,** 4717-4726 (2010)

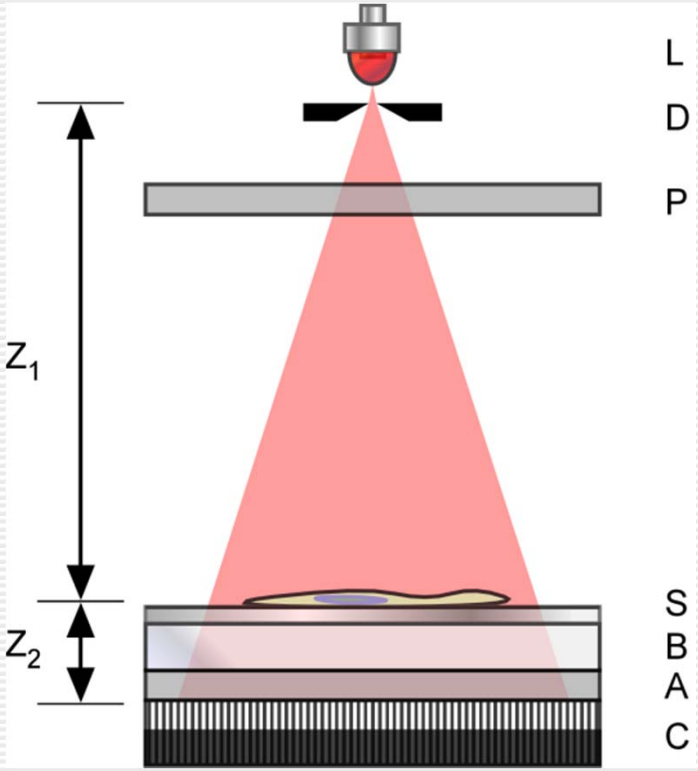

DIC microscopy by lensless holographic imaging. L: incoherent light source; D: large aperture pinhole (50~100 um); P: polarizer; S: sample on glass; B: uniaxial birefringent crystal; A: analyzer; C: CCD array. z_1 (5~10 cm) is much larger than z_2 (~1 mm). The orientation of the first polarizer is adjusted to control the differential phase contrast while the analyzer is fixed at ~45 deg. with respect to the birefringent crystal orientation.

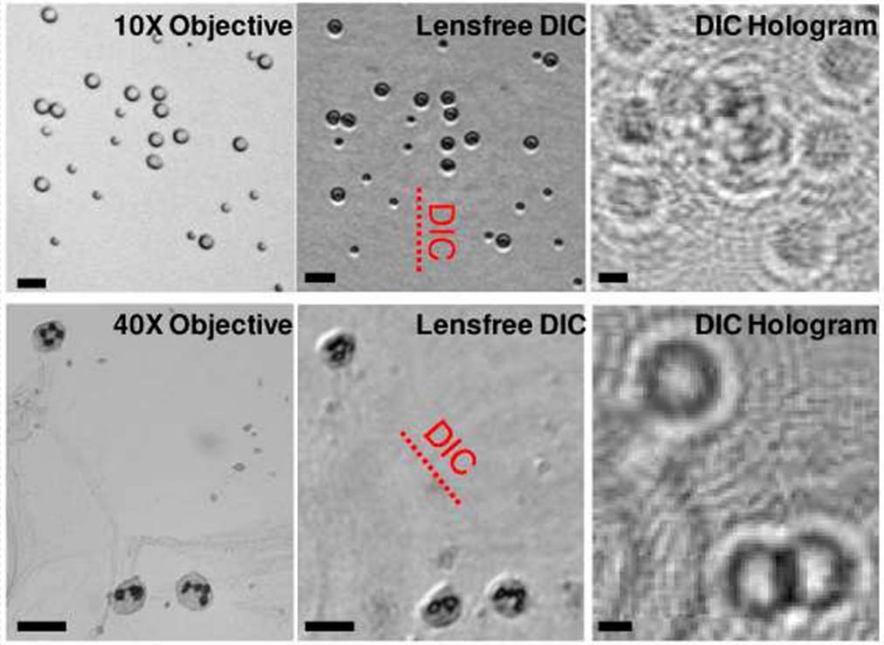

Reconstructed lensless DIC images of micro-objects. Top Row: 5 & 10 μm sized melamine (n = 1.68) beads in a medium (n = 1.524, Norland Optical Adhesive 65). The sample was illuminated at 550 nm (~18 nm FWHM bandwidth). A 50 μm aperture (at $z1$ = 10 cm) and 0.18 mm-thick quartz plate (δ ~1 μm) were used. Bottom Row: White blood cells in a blood smear sample are imaged. The sample was illuminated at 670 nm (~18 nm FWHM bandwidth) through a 50 μm aperture ($z1$ = 10 cm) and 0.3 mm-thick quartz plate (δ ~2 μm) was used for the DIC image. The shear directions are indicated in the figures with dashed lines. Conventional bright-field microscope images of the same FOV are presented for comparison. The scale bars are 20 μm.

Conoscopic Holography

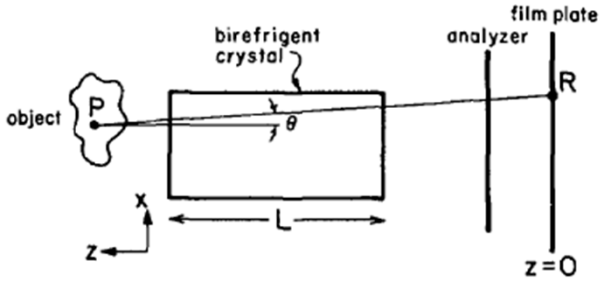

Propagation of light in a birefringent crystal.

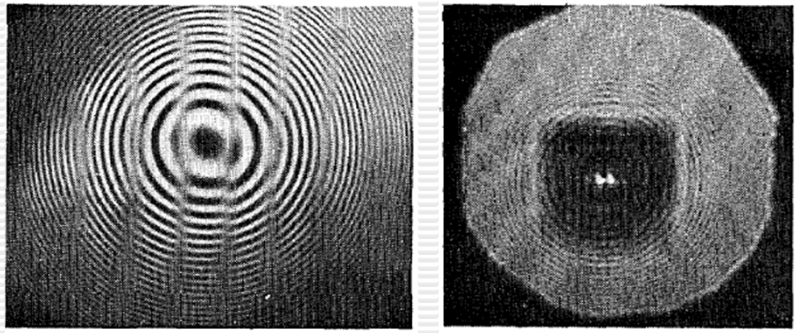

G. Sirat, and D. Psaltis, "Conoscopic Holography," Optics Letters 10, 4-6 (1985)

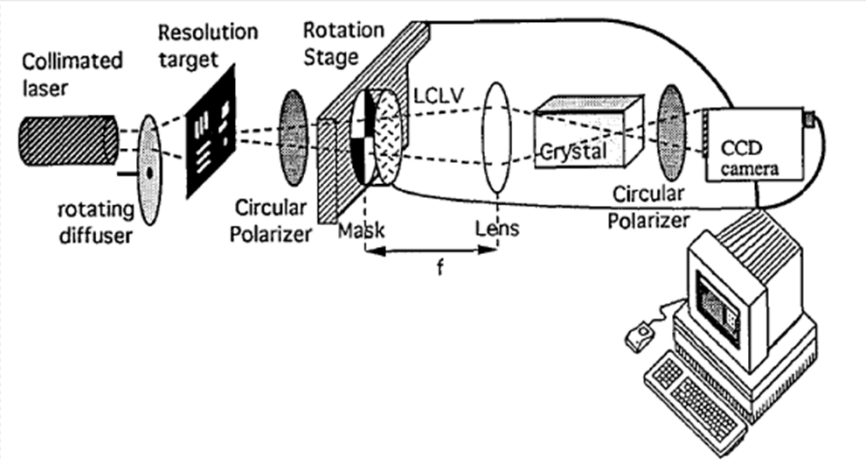

Fig. 2. Experimental setup for the acquisition of two-dimensional objects.

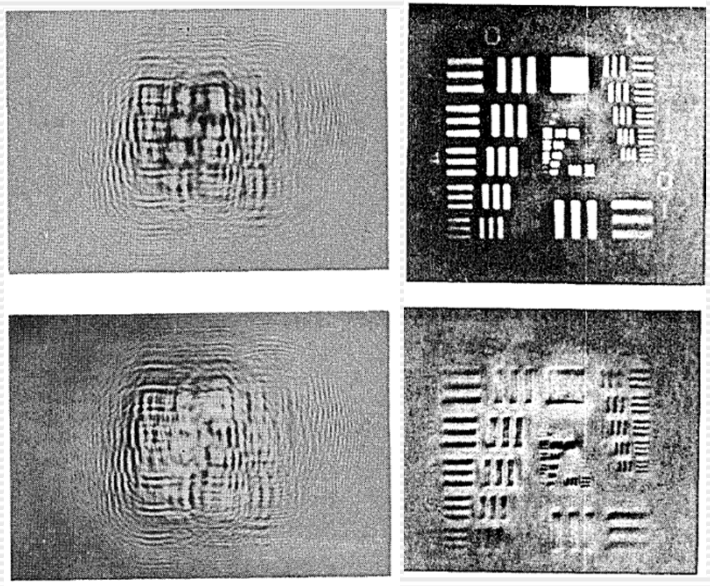

L. M. Mugnier, G. Y. Sirat, and D. Charlot, "Conoscopic holography: two-dimensional numerical reconstructions," Opt. Lett. 18, 66-68 (1993).

FINCH: Fresnel incoherent correlation holography

- J. Rosen, and G. Brooker, "Digital spatially incoherent Fresnel holography," Optics Letters **32,** 912-914 (2007).

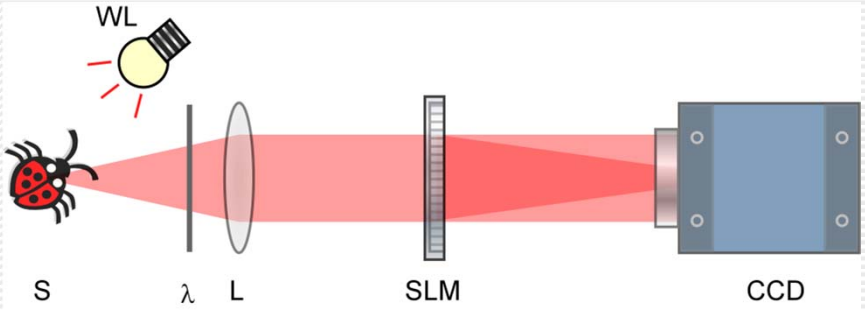

FINCH optical setup. WL: white light source; S: sample object; l: color filter; L: lens; SLM: spatial light modulator; CCD: camera

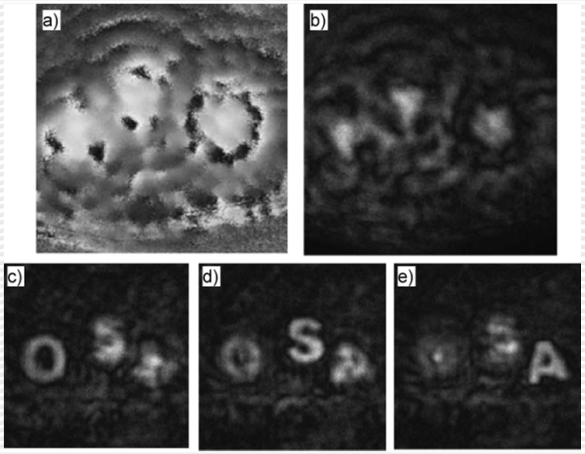

Holographic imaging of 3D objects under white light illumination by FINCH. a) Amplitude and b) phase of the complex hologram. Panels c), d), and e) show reconstruction at different distances

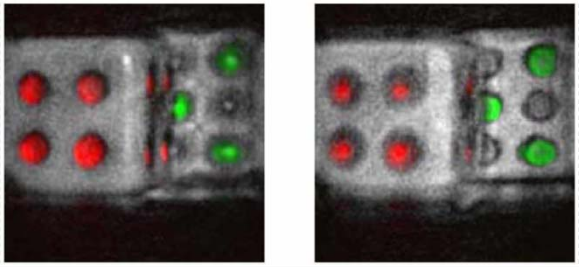

Holographic imaging of fluorescent color 3D objects by FINCH [J. Rosen, and G. Brooker, "Fluorescence incoherent color holography," Optics Express 15, 2244-2250 (2007)]

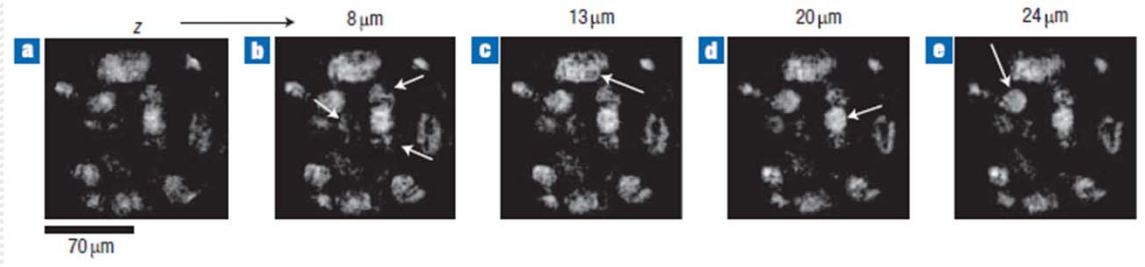

[J. Rosen, and G. Brooker, "Non-scanning motionless fluorescence three-dimensional holographic microscopy," Nat. Photonics 2, 190-195 (2008)]

FPM: Fourier Phase Microscopy

- G. Popescu, L. P. Deflores, J. C. Vaughan, K. Badizadegan, H. Iwai, R. R. Dasari, and M. S. Feld, "Fourier phase microscopy for investigation of biological structures and dynamics," Optics Letters **29,** 2503-2505 (2004)

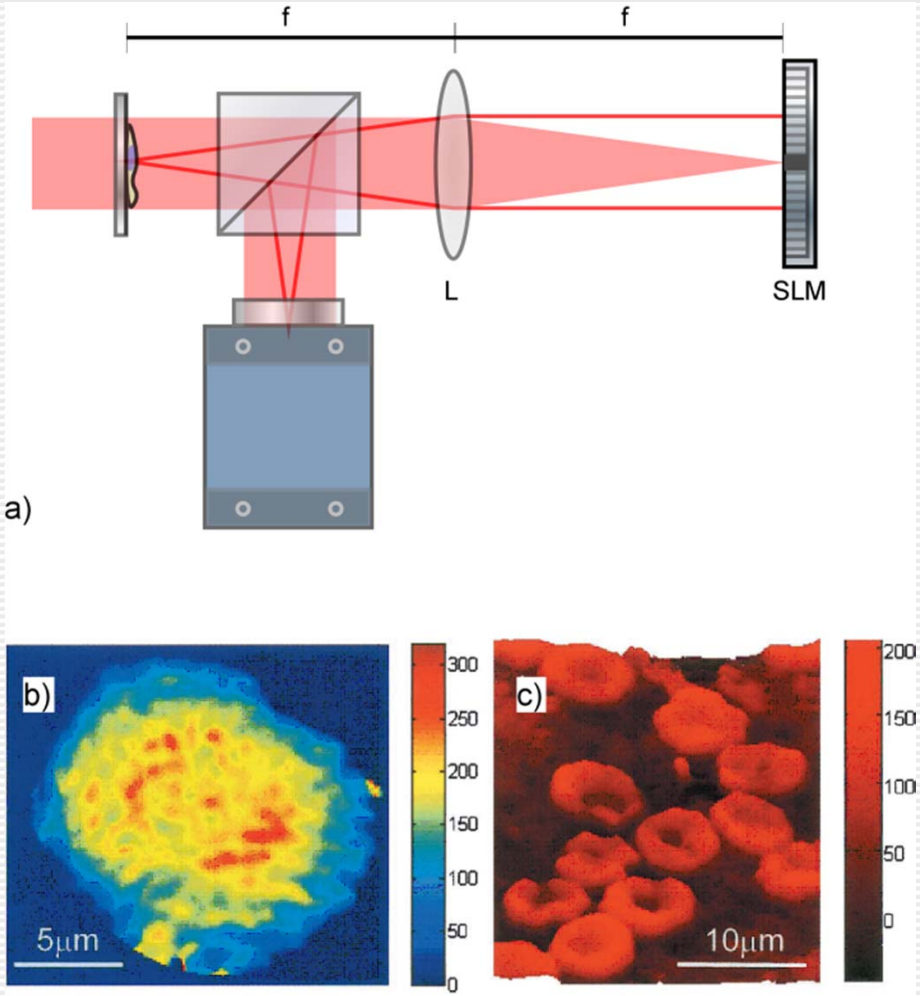

a) Fourier phase microscope. L: Fourier transform lens; SLM: spatial light modulator.
b) FPM image of a HeLa cell undergoing mitosis. c) Whole blood smear. The color bars represent optical path length in nanometers.

space time digital holography

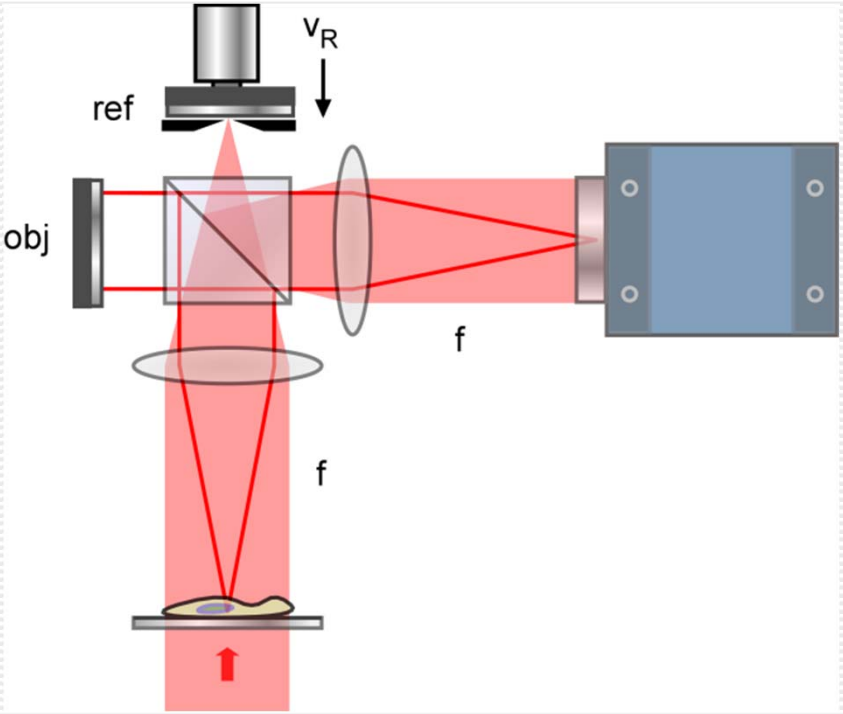

Spatio-temporal holography. The object and the camera are at focal distance from the respective lenses, as well as the object and reference mirrors. The object mirror forms an image of the object at the camera, whereas the pinhole aperture on the reference mirror performs a spatial filtering. The reference mirror is z-scanned at a constant speed.
[G. Indebetouw, and P. Klysubun, "Space-time digital holography: A three-dimensional microscopic imaging scheme with an arbitrary degree of spatial coherence," Applied Physics Letters 75, 2017-2019 (1999)]

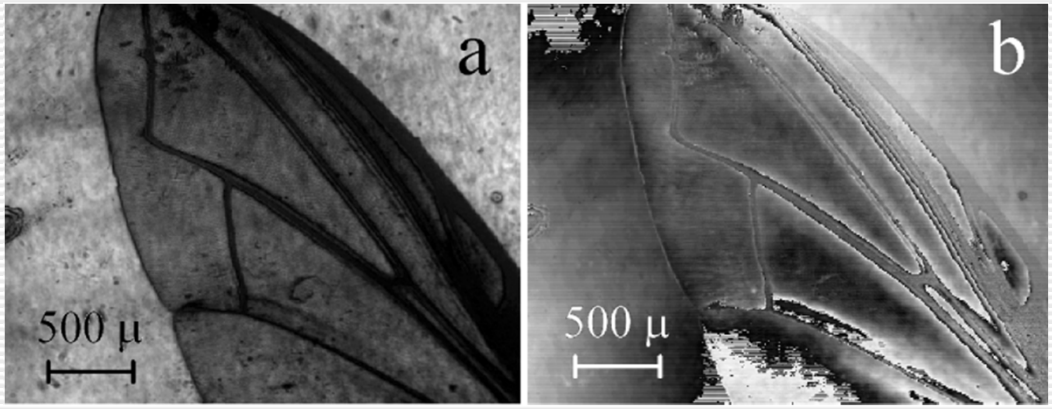

Reconstructed wave front of a fly wing recorded behind a diffuser. a) amplitude; b) phase
[G. Indebetouw, and P. Klysubun, "Imaging through scattering media with depth resolution by use of low-coherence gating in spatiotemporal digital holography," Optics Letters 25, 212-214 (2000).]

DPM: diffraction phase microscopy

- G. Popescu, T. Ikeda, R. R. Dasari, and M. S. Feld, "Diffraction phase microscopy for quantifying cell structure and dynamics," Optics Letters **31,** 775-777 (2006)

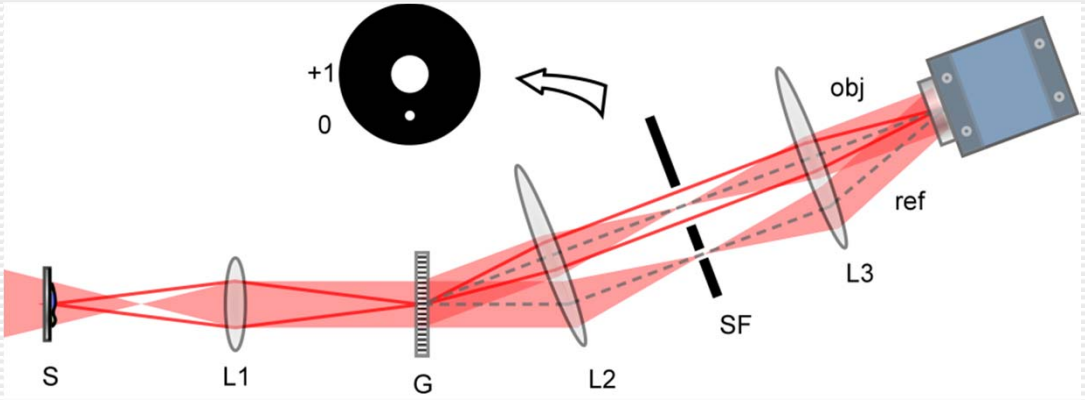

Optical system for diffraction phase microscopy. S: sample; L1: imaging lens; G: grating; L2: Fourier transform lens; SF: spatial filter; L3: inverse Fourier transform lens.

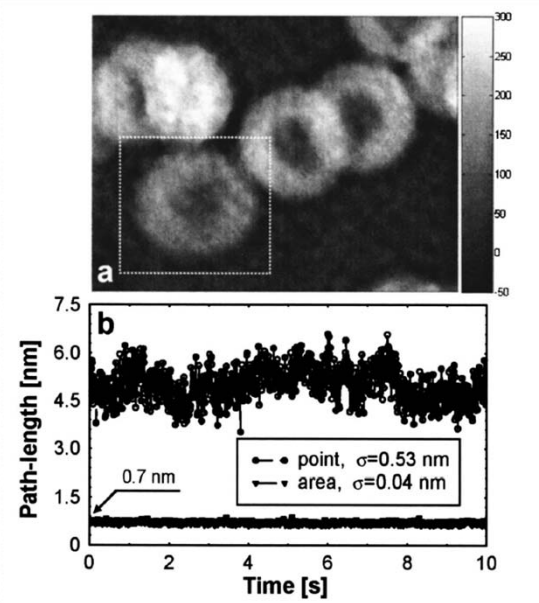

Fig. 2. a, Quantitative phase image of whole blood smear. The gradient bar represents the optical path length in nanometers. b, Temporal fluctuations of the spatial standard deviation associated with the no-sample field of view and of a single point (P) in the field of view, as indicated. The temporal standard deviations, σ, for these two signals are also shown.

quantitative differential interference contrast

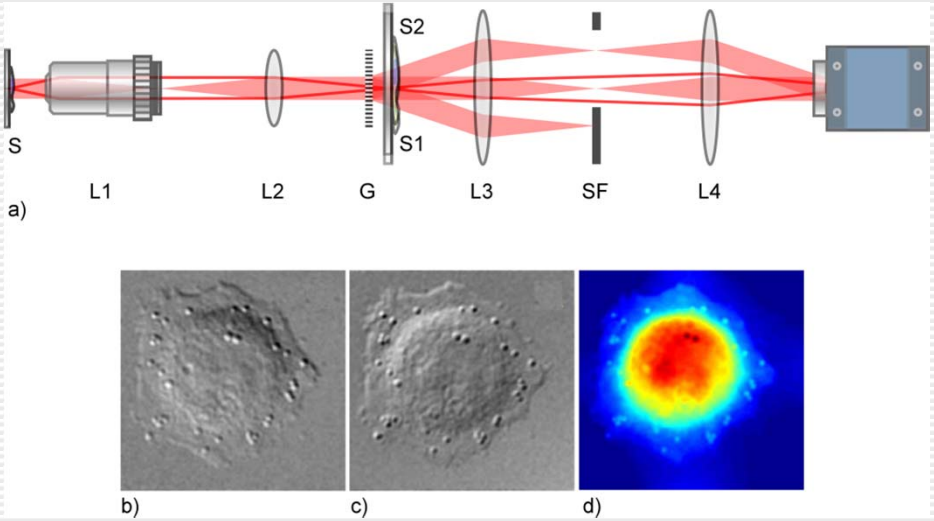

a) Quantitative DIC optical setup. S: sample; L1: objective lens; L2: relay lens; G: Ronchi grating; S1 and S2: intermediate image plane containing two (or more) laterally shifted images of the sample; L3 and L4: Fourier transform lens pair.
b) and c) A pair of DIC images of a HeLa cell reconstructed from a single exposure hologram.
d) 2D unwrapped phase image obtained by spiral integration.
[D. Fu, S. Oh, W. Choi, T. Yamauchi, A. Dorn, Z. Yaqoob, R. R. Dasari, and M. S. Feld, "Quantitative DIC microscopy using an off-axis self-interference approach," Optics Letters 35, 2370-2372 (2010).]

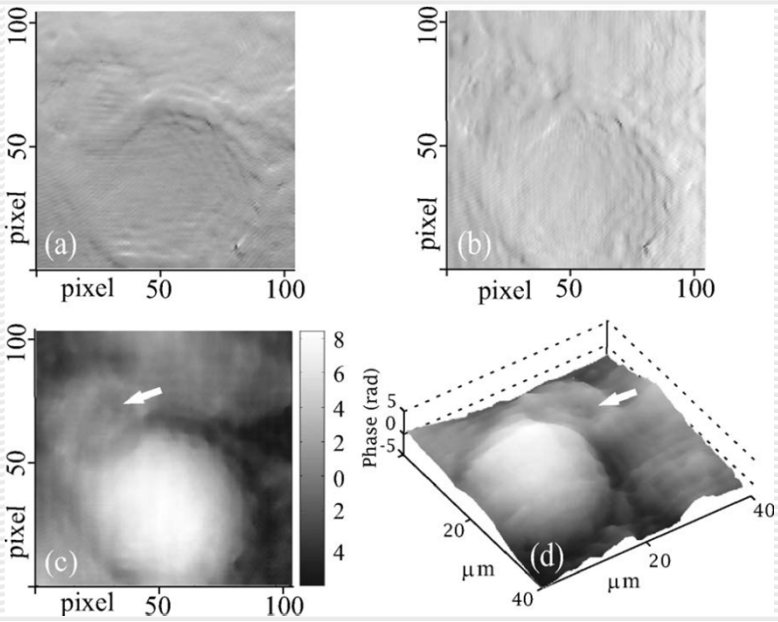

Shearograms of a mouse cell along a) *x* and b) *y* directions. c) 2D phase profile and d) its pseudo-3D rendering.
[P. Ferraro, D. Alferi, S. De Nicola, L. De Petrocellis, A. Finizio, and G. Pierattini, "Quantitative phase-contrast microscopy by a lateral shear approach to digital holographic image reconstruction," Optics Letters 31, 1405-1407 (2006)]

OSH: Optical Scanning Holography

- T. C. Poon, "Scanning Holography and Two-Dimensional Image-Processing by Acoustooptic 2-Pupil Synthesis," Journal of the Optical Society of America a-Optics Image Science and Vision **2,** 521-527 (1985)

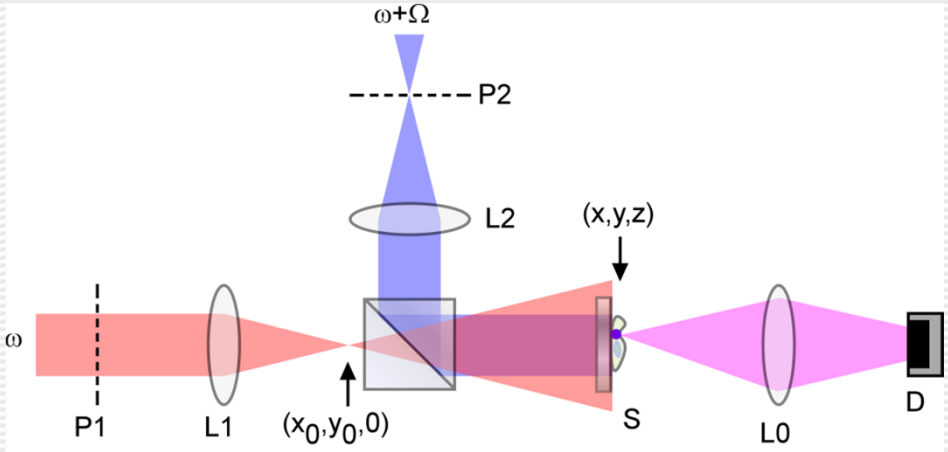

Basic OSH system optical setup. P1 and P2: pupil planes; L's: lenses; BS: beam combiner; S: sample object; D: detector

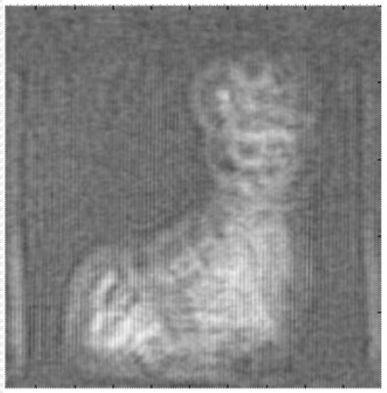

Defocused image

Focused image

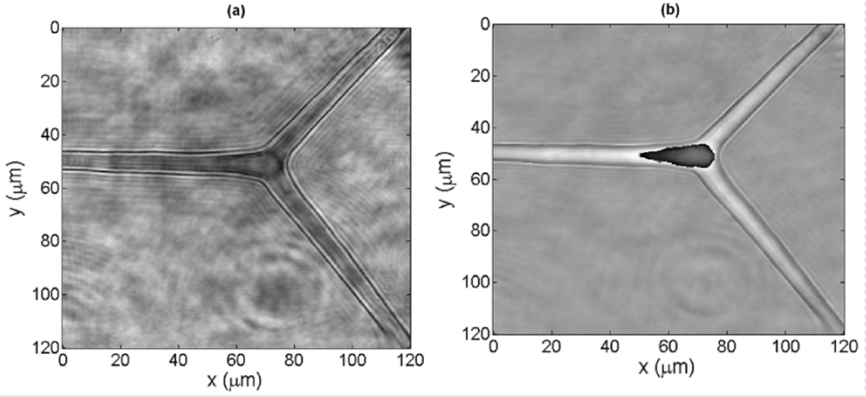

Reconstruction of a hologram recorded in coherent mode. The object is a siliceous three-pronged spongilla spicule. a) absolute value of the reconstruction amplitude; b) wrapped phase map of the optical thickness of the object relative to the mounting medium
[G. Indebetouw, Y. Tada, and J. Leacock, "Quantitative phase imaging with scanning holographic microscopy: an experimental assesment," Biomed. Eng. Online 5, 63 (2006).]

Reconstructions of the complex hologram made up from the two on-axis sine- and cosine- holograms
[T. C. Poon, "Optical Scanning Holography - A Review of Recent Progress," J. Opt. Soc. Korea. 13, 406-415 (2009).]

DIH: digital interference holography

- M. K. Kim, "Wavelength scanning digital interference holography for optical section imaging," Opt. Lett. **24,** 1693 (1999)

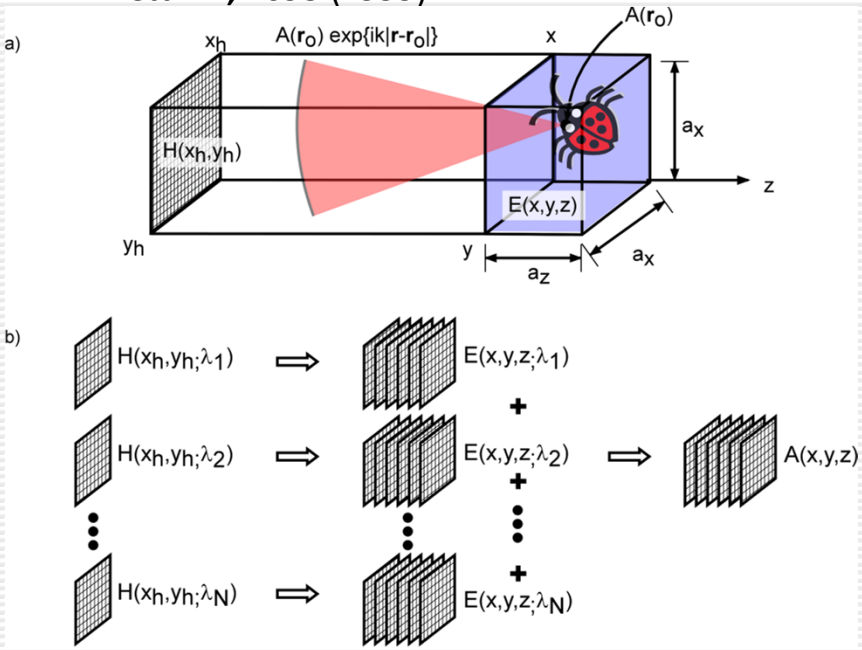

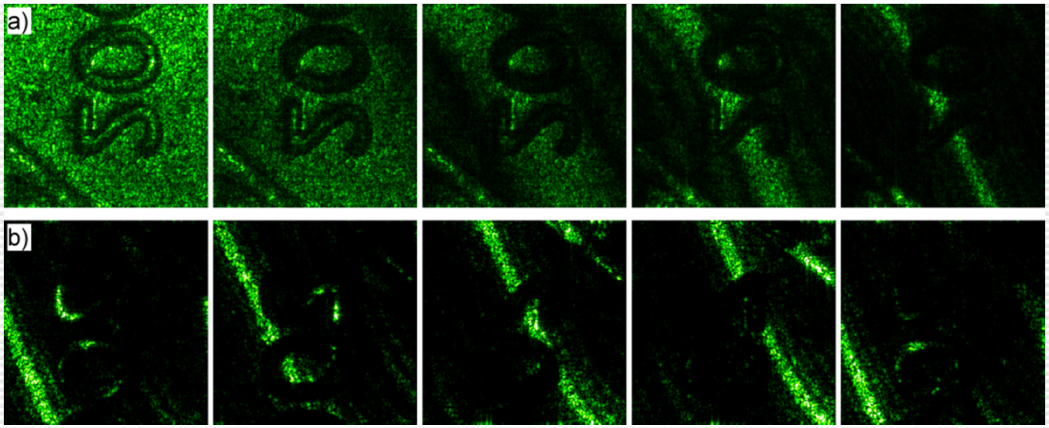

a) Buildup of axial resolution by superposition of holographic images with 1, 2, 4, 8, and 20 wavelengths.
b) Several contour images of the coin at 60 mm axial distance intervals
[L. F. Yu, and M. K. Kim, "Wavelength-scanning digital interference holography for tomographic three-dimensional imaging by use of the angular spectrum method," Optics Letters 30, 2092-2094 (2005)]

DIH

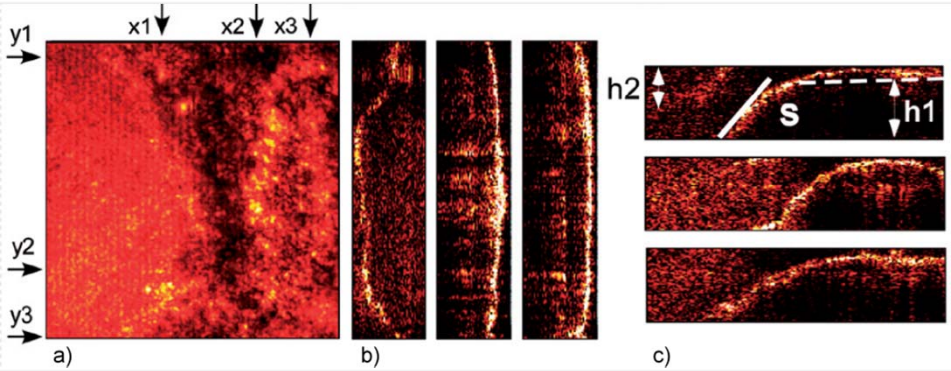

The reconstructed volume of a excised human optic nerve disk sample. The image volume is 1100 ×1100 × 280 mm^3. a) x-y flat view; b) y-z cross-sections at various x values; c) x-z cross-sections at various y values [M. C. Potcoava, C. N. Kay, M. K. Kim, and D. W. Richards, "In vitro imaging of ophthalmic tissue by digital interference holography," Journal of Modern Optics 57, 115-123 (2010)]

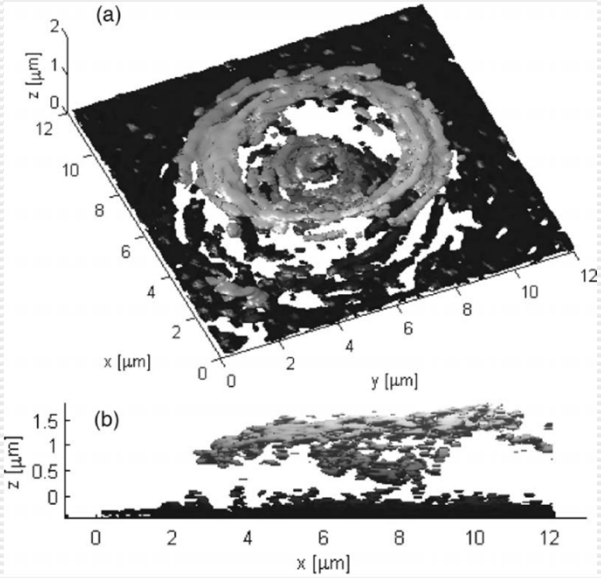

a) 3D representation of the tomography of a red blood cell; b) lateral view of a).
[J. Kuhn, F. Montfort, T. Colomb, B. Rappaz, C. Moratal, N. Pavillon, P. Marquet, and C. Depeursinge, "Submicrometer tomography of cells by multiple-wavelength digital holographic microscopy in reflection," Optics Letters 34, 653-655 (2009)]

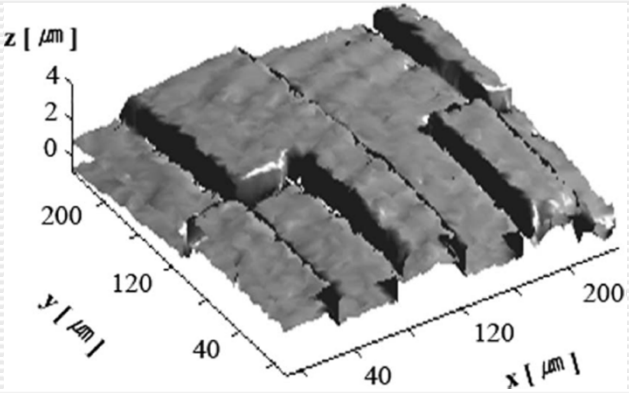

Three-dimensional rendering of a step height standard imaged by angle-scanning DIH
[Y. Jeon, and C. K. Hong, "Optical section imaging of the tilted planes by illumination-angle-scanning digital interference holography," Applied Optics 49, 5110-5116 (2010)]

OPT: optical projection tomography

- M. R. Fetterman, E. Tan, L. Ying, R. A. Stack, D. L. Marks, S. Feller, E. Cull, J. M. Sullivan, D. C. Munson, S. Thoroddsen, and D. J. Brady, "Tomographic imaging of foam," Opt. Express **7,** 186-197 (2000)
- J. Sharpe, U. Ahlgren, P. Perry, B. Hill, A. Ross, J. Hecksher-Serensen, R. Baldock, and D. Davidson, "Optical projection tomography as a tool for 3D microscopy and gene expression studies," Science **296,** 541-545 (2002)

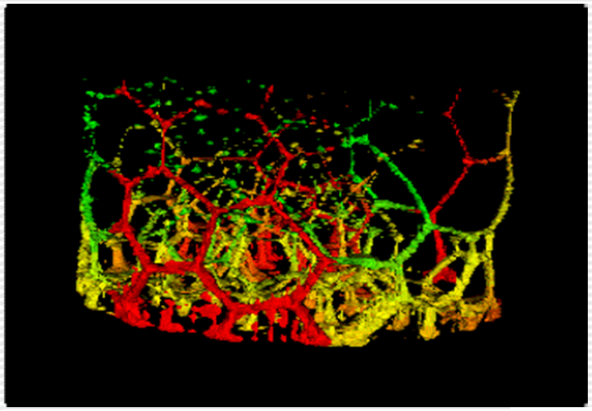

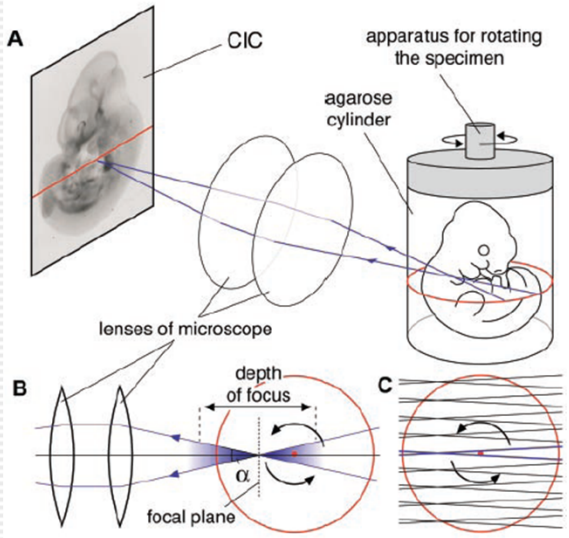

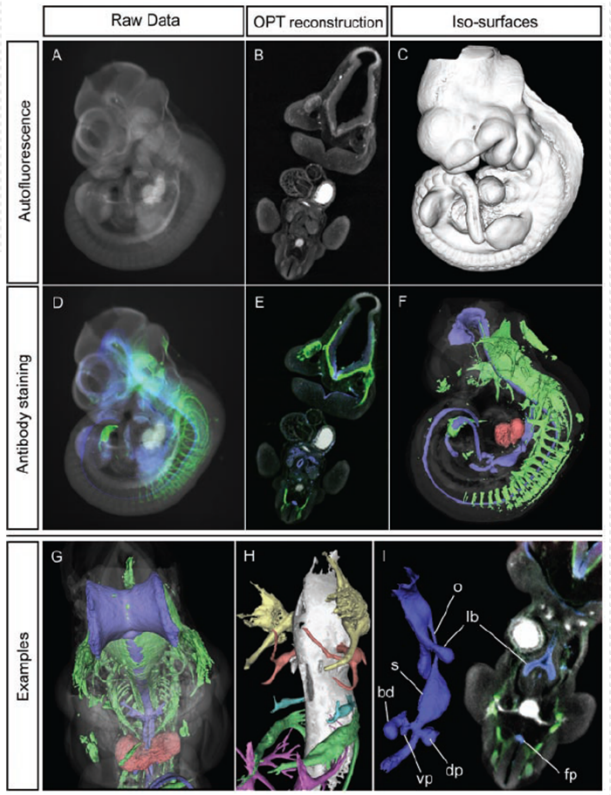

ODT: optical diffraction tomography

- F. Charriere, N. Pavillon, T. Colomb, C. Depeursinge, T. J. Heger, E. A. D. Mitchell, P. Marquet, and B. Rappaz, "Living specimen tomography by digital holographic microscopy: morphometry of testate amoeba," Optics Express **14,** 7005-7013 (2006)

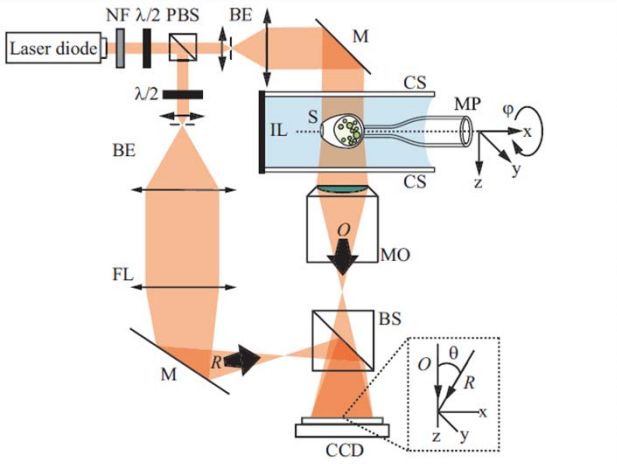

Fig. 2. Holographic microscope for transmission imaging: NF neutral density filter: PBS polarizing beam splitter: BE beam expander with spatial filter: λ/2 half-wave plate: MO microscope objective: FL field lens: M mirror: BS beam splitter: *O* object wave: *R* reference wave: MP micropipette: CS coverslip: S specimen: IL immersion liquid. Inset: a detail showing the off-axis geometry at the incidence on the CCD.

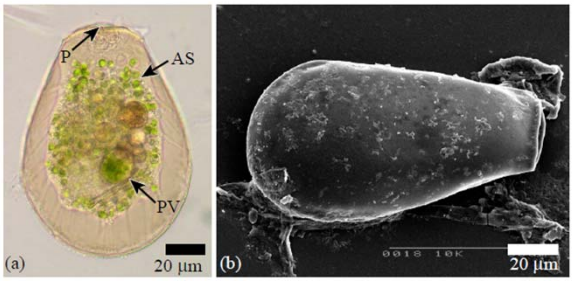

Fig. 1. Images of the testate amoebae *Hyalosphenia papilio*: (a) bright-field microscope image illustrating the amoeba itself and its content, P pseudostome (opening through which the amoeba pseudopods emerge), AS algal symbionts, PV phagocytic vacuoles; (b) SEM image illustrating the shell.

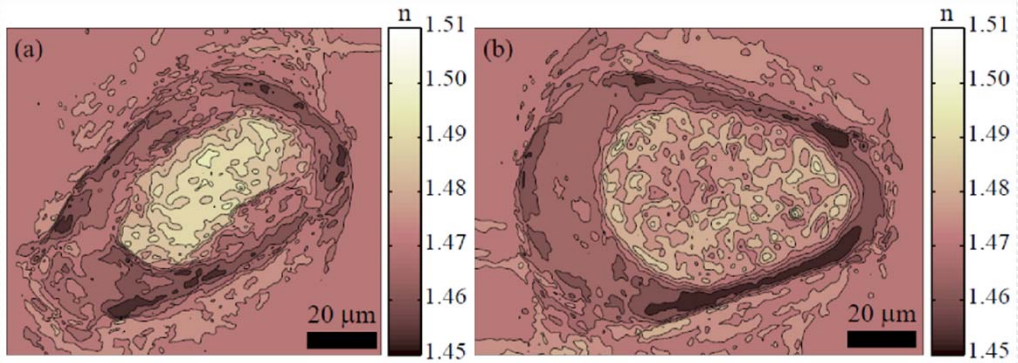

Cuts in the tomographic reconstructions of 2 different *Hyalosphenia papilio*. Discrete values of the measured refractive index *n* are coded in false colors, the color-coding scales being displayed on the right part of each corresponding cut.

- MK Kim, *Digital Holographic Microscopy: Principles, Techniques, and Applications,* Springer, 2011, ISBN: 978-1-4419-7792-2

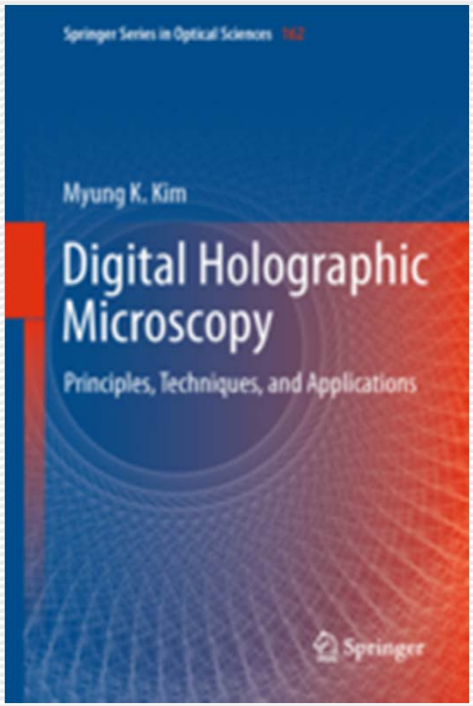

- M.K. Kim, "Principles and techniques of digital holographic microscopy," SPIE Reviews 1, 018005-1~50 (2010) (invited review paper) http://dx.doi.org/10.1117/6.0000006

conclusions

- resolve limitations of real space holography
- real time quantitative imaging
- holography with incoherent light
- integration with 3D displays
- new application areas beyond metrology and microscopy

THANK YOU